Journal of Advanced Research 47 (2023) 57–74

Contents lists available at ScienceDirect

Journal of Advanced Research

journal homepage: www.elsevier.com/locate/jare

Original Article

Advanced 3D dynamic culture system with transforming growth factor-β3 enhances production of potent extracellular vesicles with modified protein cargoes via upregulation of TGF-β signaling

Kyung Min Lim [a,f,1], Sehee Kim [a,1], Jeonghun Yeom [b,1], Yujin Choi [a], Yoonjoo Lee [a], Jongyub An [a], Minchan Gil [a], Ahmed Abdal Dayem [a], Kyeongseok Kim [a], Geun-Ho Kang [a,f], Aram Kim [c], Kwonho Hong [a], Kyunggon Kim [b,d,e,*], Ssang-Goo Cho [a,f,*]

[a] Department of Stem Cell & Regenerative Biotechnology and Institute of Advanced Regenerative Science, Konkuk University, 120 Neungdong-ro, Gwangjin-gu, Seoul 05029, Republic of Korea
[b] Convergence Medicine Research Center, Asan Institute for Life Sciences, Asan Medical Center, 88-gil, 43 Olympic-ro, Songpa-gu, Seoul 05505, Republic of Korea
[c] Department of Urology, Konkuk University Medical Center, Konkuk University School of Medicine, Seoul 05029, Republic of Korea
[d] Biomedical Research Center, Asan Institute for Life Sciences, Asan Medical Center, 88-gil, 43 Olympic-ro, Songpa-gu, Seoul 05505, Republic of Korea
[e] Department of Convergence Medicine, University of Ulsan College of Medicine, 88-gil, 43 Olympic-ro, Songpa-gu, Seoul 05505, Republic of Korea
[f] R&D Team, StemExOne Co., Ltd., 303, Life Science Bldg, 120, Neungdong-ro, Gwangjin-gu, Seoul 05029, Republic of Korea

HIGHLIGHTS

- Advanced technique to produce potent MSC-EVs harboring therapeutic protein content.
- Efficient EV isolation and purification, reducing the isolation time and scale of EV production based on T-a3D system.
- TGF-β signaling plays a key role in the high production of EVs with modified protein cargoes.
- Comprehensive quantitative proteomic analyses of the T-a3D spheroids and EVs.

GRAPHICAL ABSTRACT

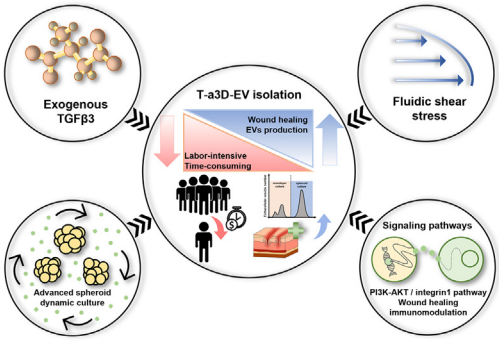

ARTICLE INFO

Article history:
Received 14 December 2021
Revised 29 June 2022
Accepted 10 September 2022
Available online 18 September 2022

Keywords:
Extracellular vesicles
MSC spheroids

ABSTRACT

Introduction: Mesenchymal stromal cells (MSCs) release extracellular vesicles (MSC-EVs) containing various cargoes. Although MSC-EVs show significant therapeutic effects, the low production of EVs in MSCs hinders MSC-EV-mediated therapeutic development.
Objectives: Here, we developed an advanced three-dimensional (a3D) dynamic culture technique with exogenous transforming growth factor beta-3 (TGF-β3) treatment (T-a3D) to produce potent MSC-EVs.
Methods: Our system enabled preparation of a highly concentrated EV-containing medium for efficient EV isolation and purification with higher yield and efficacy.
Results: MSC spheroids in T-a3D system (T-a3D spheroids) showed high expression of CD9 and TGF-β3,

Peer review under responsibility of Cairo University.

* Corresponding authors at: Department of Stem Cell & Regenerative Biotechnology and Institute of Advanced Regenerative Science, Konkuk University, 120 Neungdong-ro, Gwangjin-gu, Seoul 05029, Republic of Korea (S.-G. Cho); Convergence Medicine Research Center, Asan Institute for Life Sciences, Asan Medical Center, 88-gil, 43 Olympic-ro, Songpa-gu, Seoul 05505, Republic of Korea (K. Kim).

E-mail addresses: lmin0217@konkuk.ac.kr (K. Min Lim), worldsh80@gmail.com (S. Kim), nature8309@gmail.com (J. Yeom), trikk33@naver.com (Y. Choi), leyjo97@gmail.com (Y. Lee), delrar@naver.com (J. An), minchangil@gmail.com (M. Gil), ahmed_morsy86@yahoo.com (A. Abdal Dayem), proproggs@naver.com (K. Kim), geunhokang@naver.com (G.-H. Kang), arkim@kuh.ac.kr (A. Kim), hongk@konkuk.ac.kr (K. Hong), kkkon1@amc.seoul.kr (K. Kim), ssangoo@konkuk.ac.kr (S.-G. Cho).

[1] **These authors contributed equally**.

https://doi.org/10.1016/j.jare.2022.09.005

Advanced 3D dynamic culture with TGF-β3
TGF-β signaling
Quantitative proteomic analysis
Enhanced regenerative capacity

which was dependent on TGF-β signaling. Treatment with EVs produced under T-a3D conditions (T-a3D-EVs) led to significantly improved migration of dermal fibroblasts and wound closure in an excisional wound model. The relative total efficacy (relative yield of single-batch EVs (10–11-fold) × relative regeneration effect of EVs (2–3-fold)) of T-a3D-EVs was approximately up to 33-fold higher than that of 2D-EVs. Importantly the quantitative proteomic analyses of the T-a3D spheroids and T-a3D-EVs supported the improved EV production as well as the therapeutic potency of T-a3D-EVs.

Conclusion: TGF-β signalling differentially regulated by fluid shear stress produced in our system and exogenous TGF-β3 addition was confirmed to play an important role in the enhanced production of EVs with modified protein cargoes. We suggest that the T-a3D system leads to the efficient production of MSC-EVs with high potential in therapies and clinical development.

Introduction

Extracellular vesicles (EVs) are nano-sized membrane vesicles (50–200 nm) secreted from cells, which are required for cell–cell communication [1,2]. EVs harbor functional molecular cargoes, including both intracellular (cytoplasmic proteins and nucleic acids) and extracellular components (receptors, phospholipids, and adhesion molecules) that are protected from degradation until they reach adjacent cells. The transfer of cargo to neighboring cells affects the physiological and pathological processes.

cells, which may lead to various clinical effects [3,4]. In particular, EVs derived from mesenchymal stromal cells (MSCs) (MSC-EVs) have been investigated for the treatment of various diseases, including cardiovascular diseases, neurological dysfunction, renal disorders, and immune-related diseases [5–7].

However, most mammalian cells secrete an insufficient amount of EVs [8,9] for therapeutic applications, which is a limitation of EV-based drug development. To overcome this limitation, various culture conditions, including external stimuli-mediated activation (hypoxia, lipopolysaccharides, or thrombin) [10–12] and three-dimensional (3D) culture systems have been used to enhance the production of EVs [13–16]. Compared with conventional two-dimensional (2D) culture methods, 3D culture systems can support the self-assembly of MSCs into tightly packed clusters (MSC spheroids) with a better "*in vivo*-like" microenvironment, resulting in the improved preservation of MSC phenotype and innate properties [17–19]. Importantly, MSCs cultivated as spheroids have been reported to show substantially increased secretion of EVs [13,15,20] which may be important for enhanced regenerative and immunomodulatory effects [21,22].

During the 3D dynamic culture of MSCs for the large-scale production of EVs, mechanical forces applied to MSC spheroids were reported to modulate multiple signaling pathways via alterations in MSC morphology, mechanical stress, cell–cell or cell-extracellular matrix (ECM) adhesion capacity, and subsequent conformational changes of cytoskeletal complexes [23–25]. In our previous study, we revealed that mechanical forces induced by shear stress (hydrodynamic shear stress applied by repeated shaking and suspension) can play an important role in the regulation of self-renewal signaling pathways through the upregulation of shear stress-related genes (Egr1, Ap1, Epcam, Klf8, and Klf2) [26]. In fact, the typical shear stress is 15–20 dyne/cm^2 for arterial circulation and 1–6 dyne/cm^2 for venous circulation [27–29]. Additionally, we confirmed that the mechanical force with 60 rpm of orbital shaking *in vitro* led to the induction of self-renewal signaling pathways. We also found that the shear stress-related signaling pathway can regulate transforming growth factor beta (TGF-β) signaling as well as mechanical force-related signaling [30,31]. Recently, our previous study showed that physical mechanical forces can be converted into TGF-β-mediated biochemical signals by regulating the release of active TGF-β from the ECM [32]. In tissues exposed to various levels of mechanical forces, the amount of active TGF-β was directly related to the degree of mechanical force, implying that TGF-β/Smad2/3-mediated signaling may be one of the key pathways for the translation of physical force into biochemical signals. Similarly, human endothelial cells under shear stress conditions showed enhanced expression of TGF-β3 and endothelial cell-specific knockdown of TGF-β3, unlike TGF-β1, resulting in increased cell death, suggesting that TGF-β3 may play an important role in mechanical force-related maintenance of endothelial cells [33,34]. In addition, a recent study revealed that MSC spheroids significantly increased the secretion of TGF-β1 (10-fold) and TGF-β3 (40-fold) in a dynamic culture system [35]. Based on these reports, we hypothesized that the fluid shear stress-modulating dynamic condition with exogenous TGF-β, especially TGF-β3, could efficiently modulate the properties of MSC spheroids and their EV production capacity.

In this study, we first attempted to develop an advanced 3D dynamic culture (a3D) system for effective fluid shear stress-modulating dynamic MSC spheroid culture, optimizing the system to maintain homogeneous MSC 3D spheroids without agglomeration under our efficient shear stress induction method. Moreover, we attempted to modulate mechanical force-related regulation by inducing TGF-β signaling. We found that we could dramatically enhance the production of MSC spheroids-derived EVs through the advanced 3D dynamic culture system with an additional TGF-β3 treatment (T-a3D), and the EVs produced by our T-a3D system (T-a3D-EVs) showed apparently enhanced *in vitro* and *in vivo* therapeutic potential with high regeneration and immune-modulation capacities. To explain the enhanced production of EVs with augmented therapeutic potential in our T-a3D system, we also performed comprehensive proteomic studies on the proteins from the T-a3D MSC spheroids and T-a3D EVs.

Materials and methods

Cell culture

Human Wharton's Jelly-Derived Mesenchymal Stromal Cells (WJ-MSCs) used in this study were approved by the Institutional Review Board (IRB) (7001355–202010-BR-407) of Konkuk University. WJ-MSCs were cultured in MSC medium, which is alpha-MEM (12561072, Gibco) supplemented with 10 % FBS (PS-FB1, PEAK) and 1 % penicillin/streptomycin (15140122, Gibco). The cells were incubated at 37 °C in a humidified atmosphere containing 5 % CO_2.

Generation of 3D spheroids and cultures using an orbital shaker

WJ-MSCs were isolated from human umbilical cords and cultured at a density of 5 × 10^3 cells/cm^2 for maintenance of stemness. To generate 3D spheroids, WJ-MSCs were seeded at a density of 2.5 × 10^6 cells per well in F127 (P2443, Sigma)-coated

AggreWell™ plates and incubated for 1 d in the condition of 10 % exosome-depleted FBS culture medium based on exosome depletion protocols [36], and the cell aggregates in microwell plates were transferred to a Petri dish (10090, Spl). The spheroids were maintained in alpha-MEM containing 10 % exosome-depleted FBS on a rotary shaker at 60 rpm. TGF- β3 continuously presented in the medium until day 7 in T-a3D spheroids.

Isolation and purification of EVs

The culture medium was collected on days 3, 5, and 7. EVs were isolated and purified from the cell culture supernatant using an optimized isolation protocol [37]. Briefly, the supernatant was centrifuged at 2,000 × *g* for 10 min to remove cell debris, the supernatant was transferred to a new tube, centrifuged at 10,000 × *g* for 30 min, and subsequently centrifuged at 178,000 × *g* for 2 h at 4 °C. To remove contaminants, the EVs resuspended in 10 mL PBS were centrifuged at 178,000 × *g* for 2 h at 4 °C. Furthermore, to acquire highly purified EVs, the OptiPrep™ (iodixanol) density gradient ultracentrifugation protocol was followed [38]. Iodixanol solution (0.25 M sucrose /10 mM Tris, pH 7.5) was layered every 3 mL at concentrations of 50 %, 30 %, and 10 % (w/v) solution on the tube. A density of 1 × 10^{11} particles of EVs was loaded on the bottom of the iodixanol layers (50 %) and centrifuged for 18 h at 100,000 × *g* (K-factor: 277.5) using an SW 41 Ti rotor at 4 °C. We collected 1 mL of the 10 %–30 % layer, which was expected to contain the EVs, to remove the OptiPrep solution. The EV sample was resuspended in 1 mL of PBS and centrifuged at 178,000 × *g* for 2 h at 4 °C. The final pellets were resuspended in 200 μL PBS.

Characterization of the EVs

Protein quantification of the isolated EVs was carried out using a BCA protein assay kit (Pierce, Waltham, MA, USA) according to the manufacturer's protocol. The EVs were analyzed using dynamic light scattering analysis for size distribution and with a nanoparticle tracking analyzer (NTA) NS300 (Malvern Instruments, Malvern, UK) for the number of particles. The EVs were diluted in PBS at a concentration of 1 × 10^{11} particles/mL and in the range of 20–100 particles per frame for analysis. NTA was accomplished under the following settings: gain (12), camera level (11), flow rate, and temperature (25 °C). To determine the morphology and structure, the EVs were analyzed by transmission electron microscopy at 80 kV (JEM-1010, Nippon Denshi, Tokyo, Japan). For negative staining, EVs from the final pellet (not diluted) were transferred to a copper mesh grid (Formvar/Carbon 300 Mesh, Copper_FCF300-CU) and stained with 1 % phosphotungstic acid (P4006, Sigma) or 1 % uranyl acetate *(NC0788109, fisher scientific)*.

Western blot analysis

MSCs and EVs were dissolved in RIPA buffer (CBR002, LPS solution) containing a protease inhibitor cocktail (78440, Invitrogen) and were centrifuged at 600 ×*g* for 10 min at 4 °C. Protein samples were separated on 4%–12% Bis-Tris Flus Gels (NW04125BOX, Invitrogen), and transferred to nitrocellulose membranes (IB23001, Invitrogen). The membranes were incubated at 4 °C overnight with the primary antibody (1:1000) and washed with 1× TBST (TLP-118.1, TrnasLab) three times. The membrane was incubated with the secondary antibody for 2 h at room temperature and then washed again with 1× TBST for 30 min. All antibodies were diluted in 1× blocking buffer (TLP-115.1G, Translab). The signal was detected by Invitrogen™ iBright™ Imagers (CL-1000) and analyzed using iBright analysis software. The primary and secondary antibodies used were directed against the following proteins: CD9 (ab263023, Abcam), CD63 (ab109201, Abcam), CD81 (sc-7637, Santa Cruz), GM130 (12480, CST), Calnexin (2679, CST) Samd2/3 (8685, CST), Phospho-Smad2/3 (8828, CST), β-actin (sc-47778, Santa Cruz), HRP-linked anti-rabbit IgG (7074, CST), and HRP-linked anti-mouse IgG (7076, CST).

Real time PCR

Total RNA was isolated from spheroids and EVs using TRIzol reagent (LaboPass, CMRZ00), according to the manufacturer's instructions. The isolated total RNA was measured using a NanoDrop (ND-ONE), and cDNA was synthesized with 2 μg total RNA. Real-time PCR was performed using a 2x master mix (EBT-1802, ELPIS BIOTECH). The results were normalized to GAPDH. The sequences of the primers used were as follows: GAPDH, 5′-GTCTC CTCTGACTTCAACAGCG-3′, 3′- ACCACCCTGTTGCTGTAGCCAA-5′; Epcam, 5′-GGGAAATAGCAAATGGACACA-3′, 3′-CGATGGAGTCCAAG TTCTGG-5′; Egr1, 5′-CTTCAACCCTCAGGCGGACA-3′, 3′-GGAAAAGC GGCCAGTATAGGT-5′; AP-1, 5′-AGCCCAAACTAACCTCACG-3′, 3′-TG CTCTGTTTCAGGATCTTGG-5′; TGF-β1, 5′-TACCTGAACCCGTGTTGC TCTC-3′, 3′-GTTGCTGAGGTATCGCCAGGAA-5′; TGF-β3, 5′-CTAAGCG GAATGAGCAGAGGATC-3′, 3′-TCTCAACAGCCACTCACGCACA-5′; CD9, 5′-TCGCCATTGAAATAGCTGCGGC-3′, 3′-CGCATAGTGGATGGC TTTCAGC-5′, OCT4, 5′-CCTGAAGCAGAAGAGGATCACC-3′, 3′-AAAG CGGCAGATGGTCGTTTGG-5′; SOX2, 5′-GCTACAGCATGATGCAG GACCA-3′, 3′- TCTGCGAGCTGGTCATGGAGTT-5′; KLF4, 5′-CATCT CAAGCACACCTGCGAA-3′, 3′- TCGGTCGCATTTTTGGCACTGG-5′; BMP2, 5′-TGTATCGCAGGCACTCAGGTCA-3′, 3′- CCACTCGTTTCTGG TAGTTCTTC-5′; BMP7, 5′-GAGTGTGCCTTCCCTCTGAACT-3′, 3′-AGGACGGAGATGGCATTGAGCT-5′; COL1A1, 5′-GATTCCCTGGACC TAAAGGTGC-3′, 3′-AGCCTCTCCATCTTTGCCAGCA-5′; COL2A1, 5′-C CTGGCAAAGATGGTGAGACAG-3′, 3′- CCTGGTTTTCCACCTTCACCT G-5′; ADAMTS5, 5′-CCTGGTCCAAATGCACTTCAGC-3′, 3′-TCGTAGG TCTGTCCTGGGAGTT-5′.

Immunofluorescent staining

For immunofluorescent staining, the spheroids were washed with PBS, fixed with 4 % paraformaldehyde, and permeabilized with 0.3 % Triton X-100 at room temperature for 30 min. The spheroids were incubated overnight with primary antibodies at 4 °C. The primary antibodies used were rabbit anti oct-3/4 polyclonal IgG (sc-9081, Santa Cruz), rabbit anti-Nanog polyclonal IgG (sc-33760, Santa Cruz), and rabbit anti-Sox-2 polyclonal IgG (sc-20088, Santa Cruz). The secondary antibody used was Alexa Fluor 546 goat anti-rabbit IgG (A11035, Invitrogen). All antibodies were diluted in a 1 × blocking buffer at a dilution of 1:100. The spheroids were stained with DAPI (4′,6-diamidino-2-phenylindole (VECTASHIELD® Antifade Mounting Medium with DAPI-[H-1200]). Fluorescence was observed using an inverted fluorescent microscope (Carl Zeiss LSM 800).

Transwell migration assay

Normal human dermal fibroblasts (C-12302, Promocell) were seeded at 5 × 10^4 cells per upper chamber permeable insert (Transwell permeable supports 0.6 mm) in 24 well plates (3422, Costar) and cultivated in serum-free medium. A serum-free medium containing EVs was added to the bottom chamber. After 24 h, the upper chamber was washed with PBS and fixed with 4 % paraformaldehyde (P2031, Biosesang) for 20 min at room temperature. The cells that migrated through the insert chamber were stained with 1 % crystal violet (V5265, Sigma). Image J software was used for quantitative migration assessment.

Wound healing assay

BALB/c-nude mice (females 20–30 g, six weeks of age) were procured from IACUC (No. KU20132-1). Mice care was carried out following international laboratory animal use and care guidelines. The excision wound was generated using an 8 mm biopsy punch (BP-80F, Kai Industries), and on day 0, we applied EVs with 1×10^9 particles per 20 μL of PBS at the wound site and the carrier control once through intradermal injection. Images of wound healing were taken every 3 days using a scale marker. The assessment of wound healing was evaluated using ImageJ software to determine the percentage of wound contraction and re-epithelization. Samples of 5 μm thickness were stained with hematoxylin and eosin (H&E). Masson's trichrome (MT) staining was performed to assess the presence of ECM in the wound regeneration tissues.

Ethics statement

The protocols used in this study were approved by the ethics committees of Konkuk University (7001355–202010-BR-407) and IACUC at Konkuk University (KU20132-1) and conformed to the principles outlined in the Declaration of Helsinki.

Results

Enhanced EV production with a3D dynamic culture condition and exogenous TGF-β3 treatment

To enhance the production of EVs from MSCs, we attempted to establish an efficient fluid shear stress-modulating dynamic MSC spheroid culture system and examined whether the 3D MSC spheroid culture condition with exogenous TGF-β3 addition could efficiently modulate the properties of MSC spheroids and their EV production capacity (Fig. 1A). Initially, we performed the following experiments to characterize the properties of stemness in human Wharton's jelly-derived mesenchymal stromal cells (WJ-MSCs). The WJ-MSCs show positive surface markers (CD73, CD90, CD105) and negative markers (CD34, CD45). They can also differentiate to trilineage (adipo-, osteo- and chondrogenesis) under certain conditions (Figure S1). Next, we tried to optimize various parameters such as the size of the spheroids, horizontal or vertical dynamic culture methods, number of spheroids per culture plate, rotation speed, and harvesting time point of the culture supernatants (Table 1). The spheroids with diameters ranging from 150 to 200 μm displayed homogeneous round shapes at 60 rpm (shear stress of approximately 4 dyne/cm^2) and all spheroids emitted stable green fluorescence with calcein-AM staining (live cells) without any red ethidium homodimer-1 (EthD-1) staining (dead cells) on days 3 and 5, and the red EthD-1 signals started to be expressed in the inner region of the spheroid on day 7 (Fig. 1B). Although the harvest of EVs was possible only once per confluence (after 3 days of 2D culture) in a culture ware with the conventional 2D culture system, continuous harvest of EVs was possible in a3D and T-a3D conditions with the change of medium until the MSC spheroids were maintained without dead cells (until approximately 7 days of a3D or T-a3D culture). Based on these results, we confirmed that the MSCs in the a3D or T-a3D system were optimized to maintain homogeneous MSC 3D spheroids without agglomeration using our efficient shear stress-induction method, and harvested EVs from the a3D MSC spheroids cultured within 7 days for the subsequent experiment.

After exposure to shear stress, the change in gene expression in WJ-MSC spheroids was investigated. The shear stress markers Egr1, Ap1, and Epcam were significantly upregulated in a3D and T-a3D spheroids compared to 2D MSCs (Fig. 1C). Moreover, 3D spheroid condition can induce differentiation capacity of stem cells [17,39]. To investigate whether our culture condition maintain the stemness of MSCs, we assessed the expression of osteogenic differentiation-related genes (BMP2, BMP7) and chondrogenic differentiation-related genes (COLA1/COL2A1, ADAMTS5). Although the differentiation related genes were upregulated in both a3D and T-a3D spheroids (Figure S2B, S2C), they also showed enhanced expression of the stemness-related genes (OCT4, SOX2, and Krüppel-like factor-4) (Figure S2A) and proteins (OCT4, SOX2, and Nanog) (Figure S2D).

Interestingly, our a3D or T-a3D conditions remarkably enhanced TGF-β expression (about 10-fold or 25-fold increase in TGF-β1 or TGF-β3 expression, respectively) on day 3, compared with TGF-β1 or TGF-β3 expression on day 3 in 2D culture (Fig. 1D). Significantly, we maintained high TGF-β1 or TGF-β3 expression levels even on day 5 with the addition of exogenous TGF-β3 in the T-a3D system, although a substantially reduced TGF-β1 or TGF-β3 expression level was measured on day 5 in the a3D system.

To investigate the effect of the a3D or T-a3D system on the production of MSC-EVs, we evaluated the expression levels of EV markers (CD9 and CD63) in MSC spheroids and assessed the number of EVs from MSC spheroids. Expression levels of CD9 and CD63 were much higher in T-a3D spheroids than in a3D spheroids or 2D (day 3) MSCs (Fig. 1E). The application of the a3D MSC spheroid culture and addition of exogenous TGF-β3 (static MSC spheroid culture) led to an increase in EV production (Fig. 1F, left panel), and a significant synergistic increase in EV production was observed with a3D MSC spheroid culture plus addition of exogenous TGF-β3 in the T-a3D system, compared to that with 2D or a3D conditions (Fig. 1F, right panel). In conventional 2D culture conditions (attached MSCs), EV production was not significantly affected by the addition of exogenous TGF-β3 (Figure S3). On average, compared with the number of EVs produced per cell in the 2D system, $\sim 1.10 \times 10^3$ EVs/cell, we could prepare substantially increased numbers of EVs produced per cell; $\sim 3.46 \times 10^3$ EVs/cell in the a3D system and $\sim 6.01 \times 10^3$ EVs/cell in the T-a3D system, suggesting that, compared to the general 2D system, approximately 2.5–3.5-fold and 4.5–6.5-fold more EVs can be prepared with the a3D or T-a3D system, respectively. Moreover, when we calculated the total numbers of EVs produced from the starting cells (single-batch) for 7 days of culture, compared those in 2D ($\sim 1.7 \times 10^{10}$ EVs/cell), we could obtain about 6-fold ($\sim 1.06 \times 10^{11}$-EVs/cell) the EVs in a3D system and approximately 11-fold ($\sim 1.99 \times 10^{11}$ EVs/cell) the EVs in T-a3D system, indicating the dramatic enhancement of the production of MSC spheroids-derived EVs through the a3D dynamic culture system and the additional TGF-β3 treatment.

Proteomic analysis of the differentially expressed proteins (DEPs) in the 2D MSCs and a3D or T-a3D MSC spheroids

To obtain insight into the cellular effect of hydrodynamic 3D culture conditions or exogenous TGF-β3 addition at the proteome level, we harvested 2D-cultured attached MSCs and a3D or T-a3D MSC spheroids (Fig. 1A). We tried to identify the differentially expressed proteins (DEPs) and found 910 significant DEPs in the 2D system versus that of the a3D system and 894 DEPs in 2D versus T-a3D systems (Fig. 2A). Of particular interest, Rab proteins and Rab-related proteins, which are related to vesicular trafficking of multivesicular endosomes (MVE), including budding and docking of vesicular transportation [40,41], were significantly overexpressed in a3D and T-a3D MSC spheroids (Fig. 2B, Supplementary Table 1). In particular, Rab27b showed a higher abundance in a3D and T-a3D MSC spheroids than in 2D MSCs, suggesting that Rab27b may have an important role in the enhanced secretion of

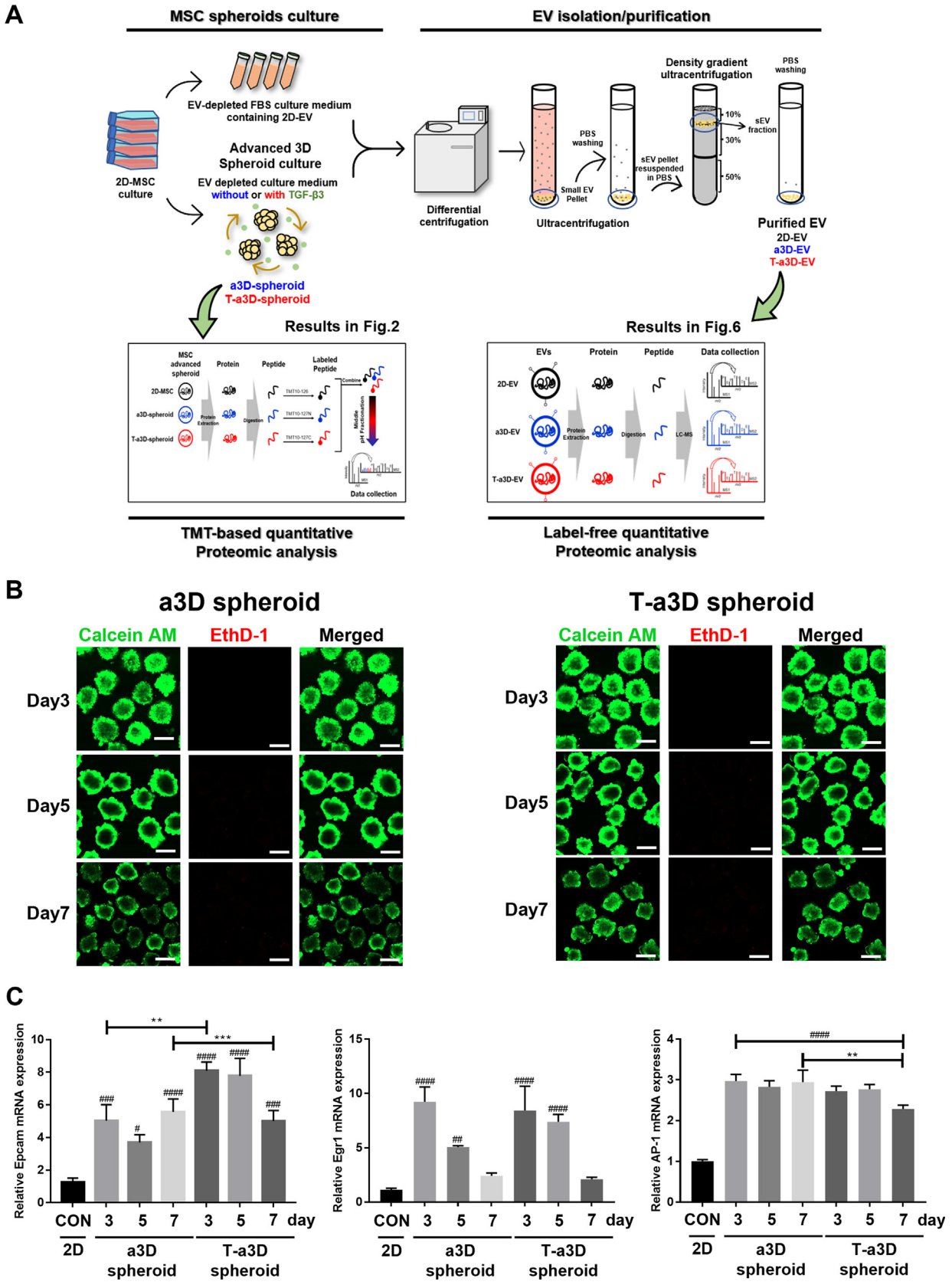

Fig. 1. *Significant elevation in the yield of EVs upon the use of an advanced 3D dynamic culture system* (A) Workflow for the proteomic analysis of spheroids and EVs under a3D or T-a3D culture system. (B) Measurements of cell viability in spheroids using advanced 3D dynamic culture system (a3D spheroid) with exogenous TGF-β3 (T-a3D spheroid) using a live (green) and dead (red) assay at days 3, 5, and 7. Scale bar: 200 μm. (C) Quantitative real-time RT-PCR analysis was performed on spheroids harvested at 3, 5 and 7 days after culture to measure the expression of shear stress-induced gene (Epcam, Egr1 and AP1). (D) Quantitative real-time RT-PCR analysis was performed on spheroids harvested at days 3, 5, and 7 after culture to measure the mRNA expression levels of TGF-β1 (left plot) and TGF-β3 (right plot). (E) Protein expression levels of CD9 and CD63 in 2D cells, a3D spheroids, and T-a3D spheroids were detected using western blots at days 3, 5, and 7, respectively. (F) Bar graphs indicate mean values of particle numbers per cell (left panel) and number of total particles of EVs (right panel). EVs were harvested at days 3, 5, and 7. Data are presented as mean ± SD (n = 6), and one-way ANOVA showed significant differences between groups, $^{**}p < 0.01$ $^{****}p < 0.0001$.

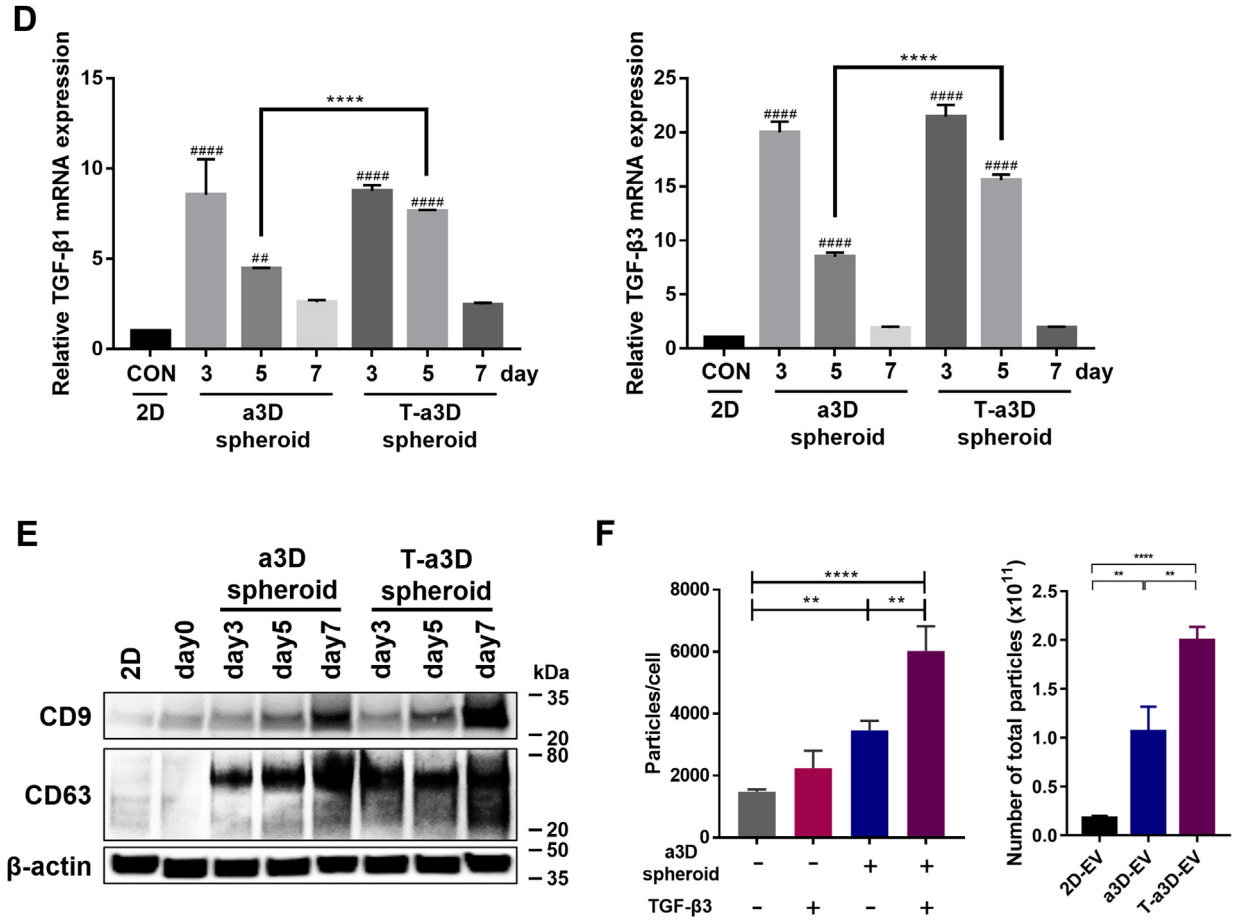

Fig. 1 (*continued*)

Table 1
Optimization of advanced 3D spheroid culture condition.

Category	Key consideration	Conditions	Advanced condition	Key consideration
Generation of spheroids	Cell seeding no./well in Agree well plate	2–3.5 × 10^6	2.5 × 10^6	Generation of spheroids without agglomeration
	Generation time of spheroids (culture time in Agree well plate)	12–24 h	24 h	
Dynamic culture	Vertical or horizontal culture	Vertical microgravity or horizontal culture	Horizontal	Maintenance of homogenous round-shaped spheroids
Cultivation of spheroids	Speed of orbital shaker	20, 50, 60 rpm	60 rpm	without agglomeration - size 150–200 μm
	Spheroid seeding no. /100 mm dish	7,000–14,000 per dish	7,000 spheroids per dish	
Harvest of EVs	Harvest time point of the spheroids culture supernatant	3,5,7 or 1,3,5,7 or 0,1,3,5,7 day	3,5,7 day	High EVs yield

EVs under 3D-culture conditions in both the a3D and T-a3D systems (Fig. 2B, Supplementary Table 1). We also detected very few DEPs ($\log_{10}$(q-value) of $\geq$ 1.3, $\log_2$ fold change ± 1) in T-a3D/a3D comparison, compared to the a3D/2D or T-a3D/2D comparison (Fig. 2A). This suggests that comparatively small amounts of DEPs induced by exogenous TGF-β3 addition can successfully enhance EV production, although the 3D-culture conditions in both the a3D and T-a3D systems may lead to a dramatic proteome change with the generation of MSC spheroids. We identified 13 significant DEPs that were dependent on exogenous TGF-β3 treatment (Fig. 2A and 2C, Supplementary Table 1). Gene ontology analysis using 13 DEPs indicated that six proteins, apolipoprotein A-I (APOA1), cysteine-rich secretory protein LCCL domain-containing 2 (CRISPLD2), hemoglobin subunit beta (HBB), lysozyme C (LYZ), serpin B3 (SERPINB3), and TGF-β3 proprotein (TGFB3)) were significantly associated with exocytosis (regulated exocytosis and exocytosis) (Fig. 2A and 2C), suggesting that the 13 DEPs, which were assumed to be directly or indirectly affected by exogenous TGF-β3, may play key roles in the substantial enhancement of EV production through the T-a3D system.

Next, as DEPs between a3D and T-a3D MSC spheroids may be important for the exogenous TGF-induced effect on EV production, we conducted affinity propagation clustering analysis to compare the proteomic contents of a3D and T-a3D MSC spheroids. We identified cluster 2, which was composed of 35 proteins, including fibronectin (FN1), TGFB3, cartilage oligomeric matrix protein (COMP), and tubulointerstitial nephritis antigen-like (TINAGL1), which significantly increased in the T-a3D condition compared to

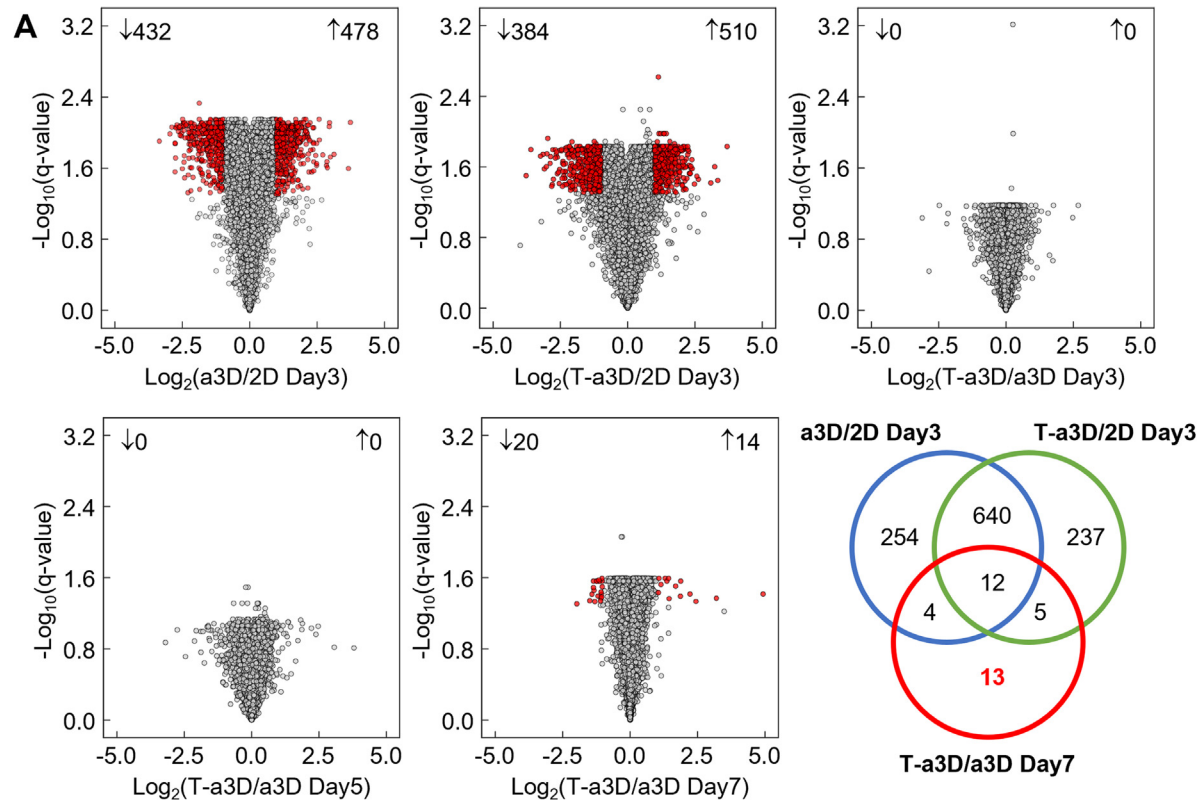
A
↓432
↑478
↓384
↑510
↓0
↑0
↓0
↑0
↓20
↑14
-Log10(q-value)
Log2(a3D/2D Day3)
Log2(T-a3D/2D Day3)
Log2(T-a3D/a3D Day3)
Log2(T-a3D/a3D Day5)
Log2(T-a3D/a3D Day7)
a3D/2D Day3
T-a3D/2D Day3
T-a3D/a3D Day7
254
640
237
12
4
5
13

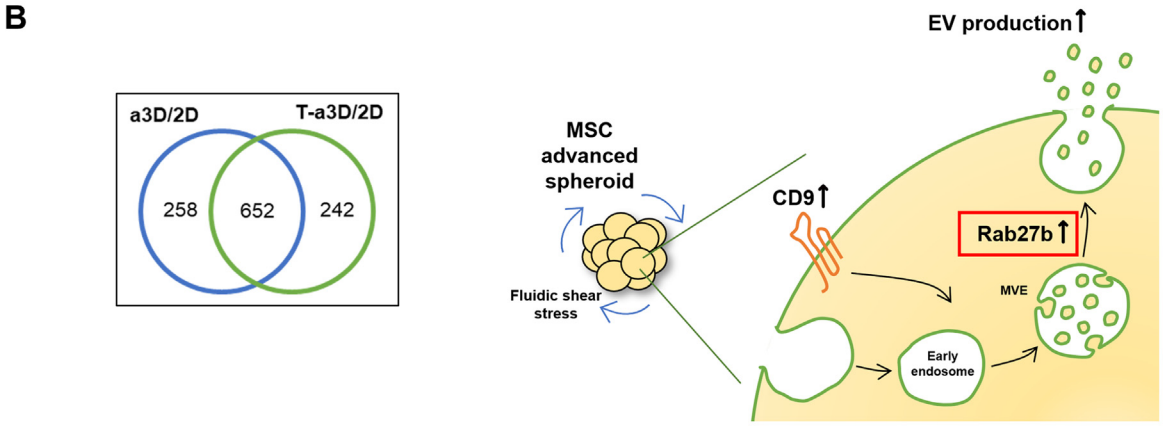
B
a3D/2D
T-a3D/2D
258
652
242
EV production
MSC advanced spheroid
Fluidic shear stress
CD9
Rab27b
MVE
Early endosome

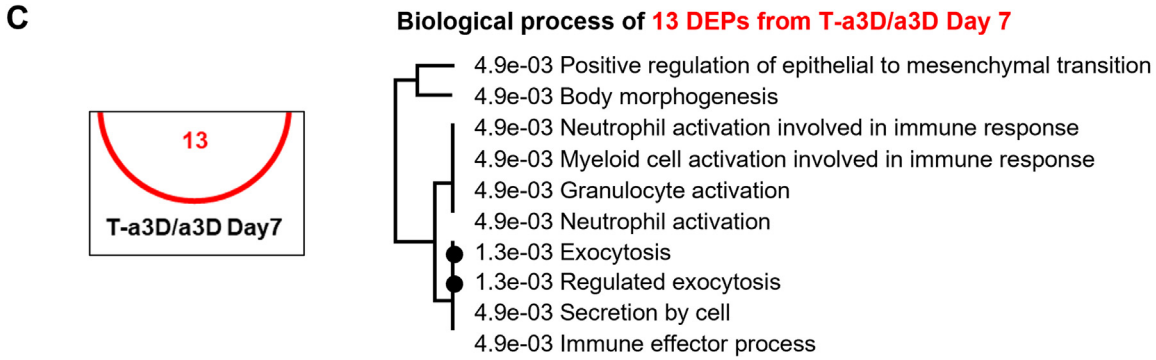
C
13
T-a3D/a3D Day7
Biological process of 13 DEPs from T-a3D/a3D Day 7
4.9e-03 Positive regulation of epithelial to mesenchymal transition
4.9e-03 Body morphogenesis
4.9e-03 Neutrophil activation involved in immune response
4.9e-03 Myeloid cell activation involved in immune response
4.9e-03 Granulocyte activation
4.9e-03 Neutrophil activation
1.3e-03 Exocytosis
1.3e-03 Regulated exocytosis
4.9e-03 Secretion by cell
4.9e-03 Immune effector process

the a3D condition, especially on the 7th day (Supplementary Table 3, Fig. 2E). Gene ontology analysis using these 35 proteins indicated that these proteins are involved in regeneration processes such as extracellular matrix organization, cell adhesion, angiogenesis, endodermal cell differentiation, positive regulation of stress fiber assembly, and gene expression (Supplementary Table 4, Fig. 2F). Of the 35 proteins identified through affinity propagation clustering analysis, FN1, TGFB3, COMP, and TINAGL1 were also identified as being among the exogenous TGF-β3 treatment-specific DEPs (Fig. 2A, 2C, 2E, Supplementary Table 1, Table 3).

Importantly, 10 proteins (agrin (AGRN), biglycan (BGN), collagen alpha-2(IV) chain (COLA4A2), COMP, elastin microfibril interfacer 1 (EMILIN-1), FN1, basement membrane-specific heparan sulfate proteoglycan core protein (HSPG2), laminin subunit gamma-1 (LAMC1), lysyl oxidase homolog 1 (LOXL1), Thrombospondin-1 (THBS1)) out of the 35 proteins were found to be specifically involved in TGF-β3-related ECM organization and extracellular structure organization (Fig. 2G), which was confirmed through a protein–protein interaction database analysis (STRING 11.0, https://string-db.org; [42]).

These results support the hypothesis that T-a3D culture conditions can enhance TGF-β3-related ECM organization, cell–cell adhesion for larger spheroid formation and translational initiation, and SRP-dependent co-translational protein targeting the membrane for increased EV production. The proteome analysis of the 2D MSCs and a3D/T-a3D MSC spheroids confirmed that the expression of CD9 and TGFβ3 was highly increased in T-a3D spheroids at days 5 and 7, compared to 2D MSCs (Fig. 2H, 2I). However, we could detect TGF-β1 in a3D and T-a3D MSC spheroids and observed very low level of TGF-β3 in a3D MSC spheroids. Although we cannot explain the exact reason, we can expect that the high TGF-β3 level in T-a3D MSC spheroids plays an important role in EV production.

TGF-β signaling-dependent increase of CD9 expression and EV production in a3D/T-a3D MSC spheroids

Importantly, we found that CD9 protein and mRNA expression were significantly suppressed upon treatment with the TGF-β receptor inhibitor SB-431542 (Fig. 3A, 3B), and the enhancement of EV production was also repressed by SB-431542 treatment in both the a3D and T-a3D systems (Fig. 3C), although SB-431542 treatment had almost no effect on the number of total proteins in MSC spheroids (Figure S4). These results suggest that TGF-β signaling may play an important role in both the approximately 2–3-fold enhancement of EV production under 3D-culture conditions in both the a3D and T-a3D systems and the other about a 2.5 % increase in EV production with exogenous TGF-β3 addition in the T-a3D system. Consistently, in the T-a3D system, we confirmed that the phosphorylation of Smad2/3 protein, which is a downstream target of canonical TGF-β signaling [43] was significantly upregulated in T-a3D spheroids and suppressed in the presence of the TGF-β receptor inhibitor SB-431542 (Fig. 3D), supporting that our advanced 3D dynamic culture system enhanced EV production by increasing the protein expression of CD9 and Rab27b through TGF-β signaling (Fig. 2D).

Characterization of EVs from 2D MSCs and a3D or T-a3D MSC spheroids

First, through western blotting, we confirmed that EV markers such as tetraspanins (CD9, CD81, and CD63) were clearly detected in all 2D-, a3D-, and T-a3D-EVs, and Golgi (GM130) or endoplasmic reticulum marker (Calnexin) were hardly observed in EVs, although they were expressed in cell lysates (CL) (Fig. 4A). Based on transmission electron microscopy (TEM) images, the 2D-, a3D-EVs and T-a3D-EVs displayed similar cup shapes (Fig. 4B). Dynamic light scattering analysis revealed that all EV samples exhibited a homogeneous size distribution, and their mean diameters were found to be 100–200 nm (Fig. 4C). Moreover, as the detailed size distributions were assessed by fractionating particles into four size ranges: <100 nm, 100–150 nm, 150–200 nm, and > 200 nm, the particles from all 2D-, a3D-, and T-a3D-EVs were determined to have similar subpopulations (Fig. 4D).

In addition, to confirm the purity of the isolated EVs, we measured the concentration of TGF-β3 in the final EVs by ELISA because we added exogenous TGF-β3 to the T-a3D system. Although exogenous TGF-β3 was added to the culture medium when we started the T-a3D culture, the residual concentration of TGF-β3 per 5×10^9 particles (same dosage for wound healing experiments) was hardly detected in T-a3D-EVs (Figure S5), suggesting that the functional activity of T-a3D-EVs will not be affected by the contamination of the exogenous TGF-β3 initially added to the T-a3D system.

The improved regeneration capacity of T-a3D-EVs

To determine the regeneration capacity of EVs, we compared the migratory effects of 2D-, a3D-, and T-a3D-EVs on human dermal fibroblasts using a Boyden chamber assay. The staining images showed that the proportion of positively stained cells was higher in the T-a3D-EVs-treated group than in the 2D- or a3D-EVs groups (Fig. 5A). The quantitative graph showed that T-a3D-EVs significantly improved the *in vitro* wound healing capacity (Fig. 5B). The relative total efficacy (relative yield of single-batch EVs (10–11-fold) × relative regeneration effect of EVs (2–3-fold)) of T-a3D-EVs was approximately up to 33-fold higher than that of 2D-EVs.

The wound closure rates were significantly increased upon T-a3D-EVs treatment, compared to the 2D-EVs or a3D-EVs (Fig. 5C, 5D) in excisional wound models. To confirm regeneration of the wound and reconstruction of the ECM, tissues obtained from EV-treated wounds were stained with hematoxylin and eosin (H&E) and Masson's trichrome (MT). The representative images revealed that T-a3D-EVs treatment led to significantly enhanced migration of dermal fibroblasts within the dermis layer and improved re-epithelialization in the epithelial layer (Fig. 5E). MT staining to evaluate matrix remodeling also showed that T-a3D-EV-treated tissues displayed improved collagen synthesis compared to 2D- or a3D-EV-treated tissues (Fig. 5F), supporting the idea that T-a3D-EVs have substantially improved regeneration capacity.

Fig. 2. *Comparative analysis of quantitative MSC spheroids proteome of the 2D, a3D, and T-a3D conditions.* (A) Volcano plots of proteomic data (protein groups were ranked according to their *q*-values [y-axis] and their relative intensity ratios [$\log_2$ fold change] between the sample types [x-axis]). Protein groups with a Benjamini–Hochberg FDR of ≤ 0.05 and $\log_2$ fold change ± 1 were considered differentially expressed (red). Arrows represent an increase or decrease compared to the base of ratio. A Venn diagram indicating the overlap between differentially expressed protein groups from WJ-MSC proteome. (B) Schematic representation of the EV biogenesis of a3D MSC spheroid. (C) Biological process enrichment analysis of the 13 significant proteins in T-a3D from DEPs. (D) Schematic representation of the EV biogenesis of T-a3D MSC spheroid. (E) Spheroid protein abundance for cluster 2 of Day 3, 5, 7 from a3D and T-a3D sets were shown as box pots, respectively. And expression level of 35 proteins in cluster 2 increase in T-a3D compared to a3D regardless culture time. (F) GO analysis (ShinyGO) of 35 proteins related to TGF-β3. (G) Interactome analysis was conducted using STRING 11.0 (https://string-db.org/) using 10 proteins from cluster 2 and result showed protein–protein interaction network related to TGF-β3 (red circle). Each line with different color between proteins indicate possible interactions (the known interactions (blue and pink), the predicted interactions (green, red, and blue) and other interactions (faint green, black, and gray), respectively). A scatter dot plot indicating distribution of intensities from CD9 (H) and TGF-β3 (I) in each sample.

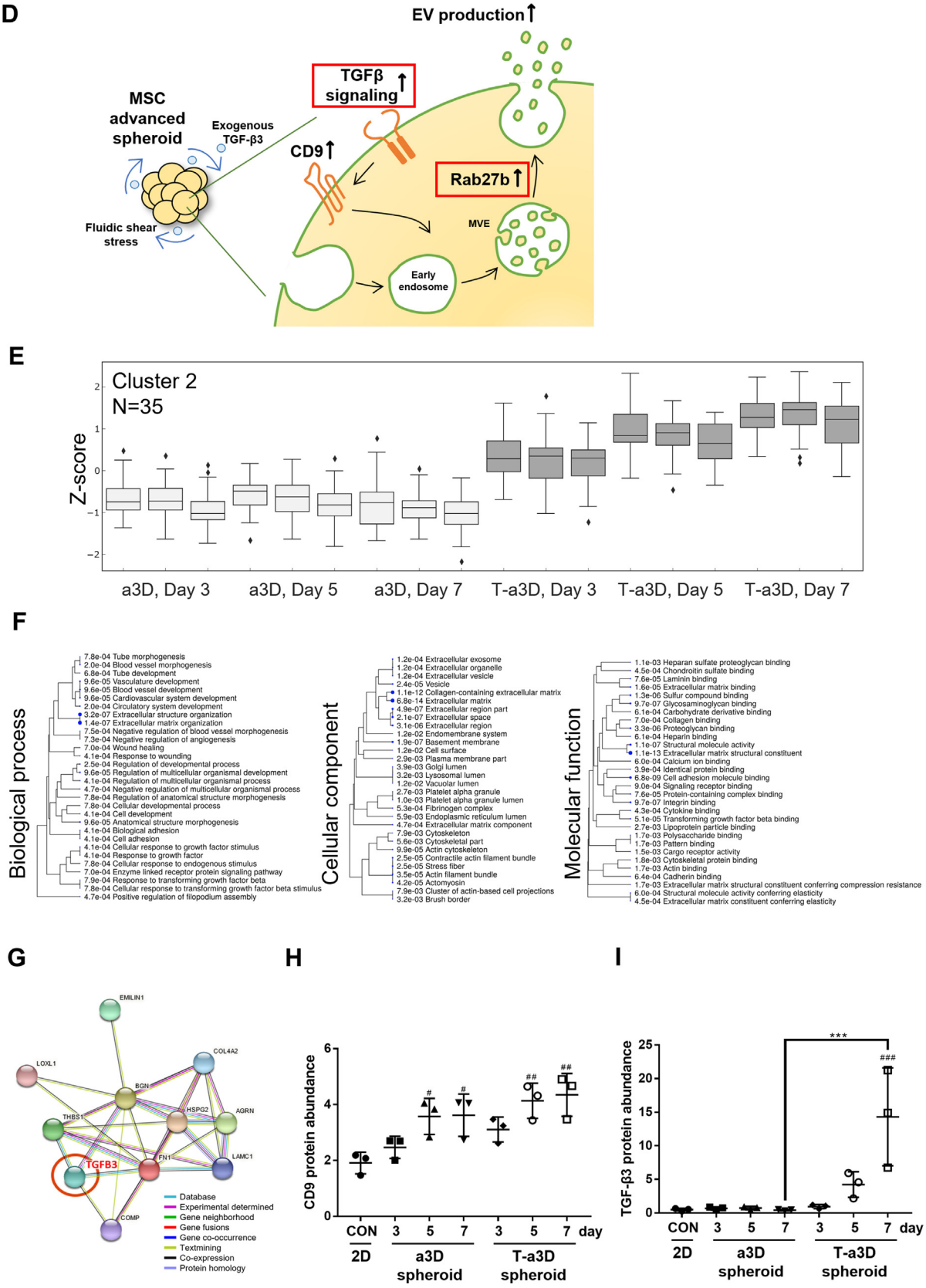

Fig. 2 (*continued*)

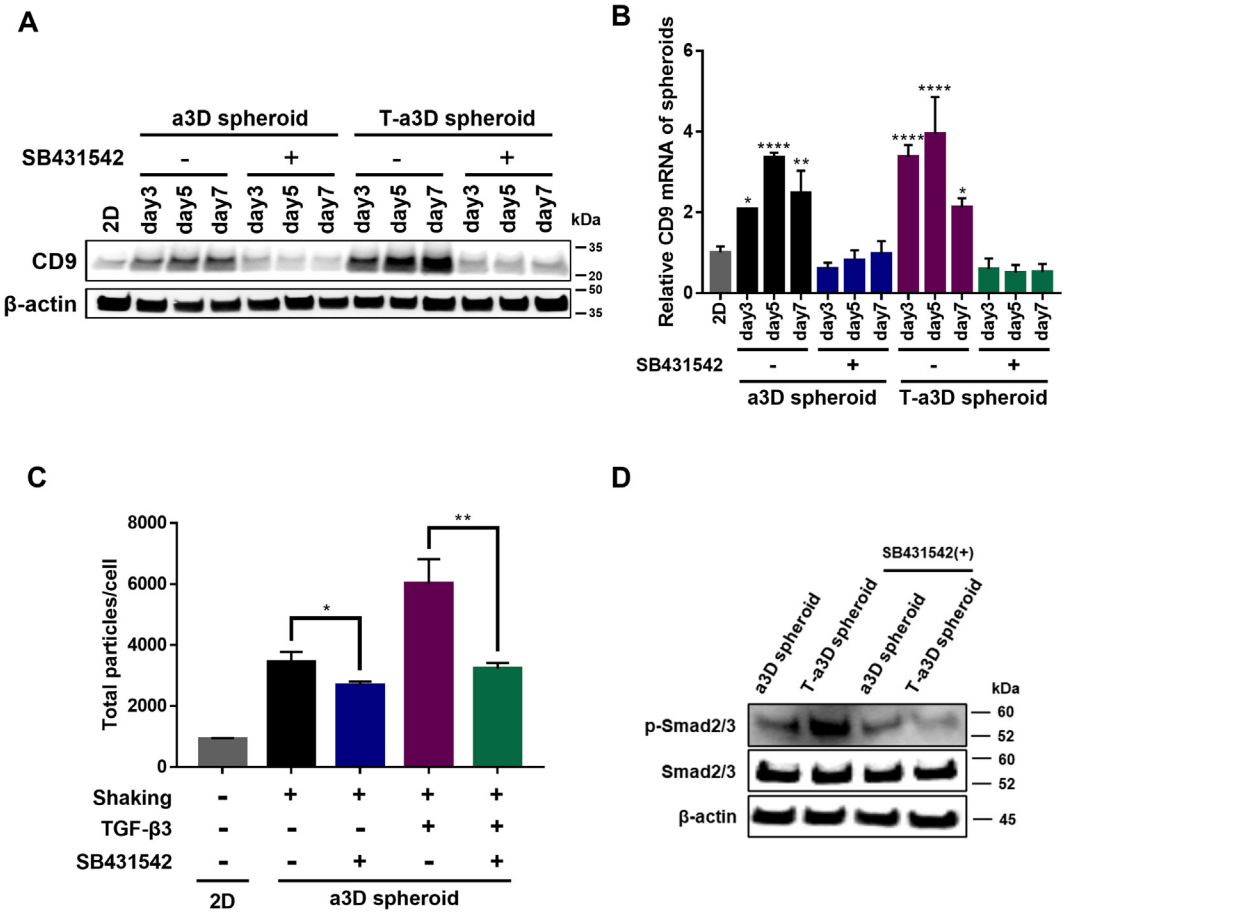

Fig. 3. *TGF-β3 receptor signaling-dependent enhancement of CD9 expression and EV production of T-a3D MSC spheroids* (A) Western blot data for the relative CD9 protein expression changes upon SB431542 treatment. (B) The quantitative real time-PCR data for the relative CD9 mRNA expression changes with SB431542 treatment. Data are presented as mean ± SD, and statistical analyses were evaluated by performing Student's *t*-test (unpaired, two-tailed); $^{*}p < 0.05$ and $^{***}p < 0.001$. (C) Comparison of EVs yield between control and SB431542-treated group. Data are presented as mean ± SD (n = 6), and one-way ANOVA showed significant differences between groups, $^{*}p < 0.05$, $^{**}p < 0.01$. (D) The protein expression of phospho-Smad2/3 and Smad2/3 in 2D cells, a3D spheroids, and T-a3D spheroids.

Proteomic analysis of 2D-, a3D-, or T-a3D-EVs

To understand the potent therapeutic function of T-a3D-EVs, the protein contents of 2D-, a3D-, or T-a3D-EVs were analyzed using LC-MS-based label-free quantification (LFQ) (Fig. 1A). First, we prepared and purified the 2D-, a3D-, and T-a3D-EVs, and the amount of EV proteins was analyzed using the BCA assay. The protein quantities of the 2D-, a3D-, and T-a3D-EVs were 33 μg, 26 μg, and 29 μg, respectively (Fig. 6A), and the abundance distribution of the proteome showed a similar pattern to the amount of protein (Figure S6A). Proteins were extracted from equal amounts of EVs (20 μg), and 394 protein groups were identified in technical triplicates (explained in detail in the "Materials and Methods" section). Among the 394 identified proteins, 138 ± 1 protein groups of 2D-EVs, 304 ± 5 of a3D-EVs, and 320 ± 14 of T-a3D-EVs were quantified (Fig. 6A, Supplementary Table 2). Among the 394 EV proteins, 44 EV protein markers among the previously known 'Top 100 EV markers' (https://exocarta.org/exosome_markers_new, [44]) were identified in all EV samples in this study, and the quantitative distribution of the EV marker proteins was observed to be very similar among the 2D-, a3D-, and T-a3D-EVs (Figure S6A). This result can be inferred to mean that the 2D-, a3D-, and T-a3D-EVs contain similar amounts of proteins, but the complexity of the proteome in a3D- and T-a3D-EVs was increased more than that in the 2D-EVs.

From the total identified proteins from three kinds of EV sample sets with triplicate runs, 394 proteins were quantified three times at each EV sample set and GO analysis using those proteins indicated that most of the proteins belonged to exosomes (Figure S6B). A larger number of proteins in the 2D-EVs were found in exosomes than in a3D and T-a3D EV sample sets. Proteins of the a3D- and T-a3D-EVs, unlike in the 2D-EVs, were found in the cytosol, nucleolus, ribosome, and ECM (Figure S6B). In addition, when comparing the data set reported in Vesiclepedia [45] with the EV proteome in our study, most proteins except for three (adipocyte plasma membrane-associated protein and prolyl 3-hydroxylase 1 in both a3D- and T-a3D-EVs, and prostaglandin G/H synthase 2 in T-a3D-EVs only in T-3D EVs) were also found in the Vesiclepedia data (Fig. 6B, Supplementary Table 2).

From the hierarchical clustering analysis using the Z-score to normalize the abundance with a Benjamini-Hochberg false discovery rate (FDR) of ≤ 0.05, we identified four clusters (Fig. 6C): Cluster 1 contained 87 proteins whose expression was high in both a3D-EVs and T-a3D-EVs, indicating that these proteins might be 3D spheroid culture-specific, Cluster 2 contained 42 proteins whose expression was high in T-a3D-EVs; Cluster 3 consisted of 23 proteins whose expression was high in a3D-EVs; and Cluster 4 had 51 proteins whose expression was high in 2D-EVs. Using the gene ontology tool, the functional characteristics of the biological process category for each cluster were investigated, and it was

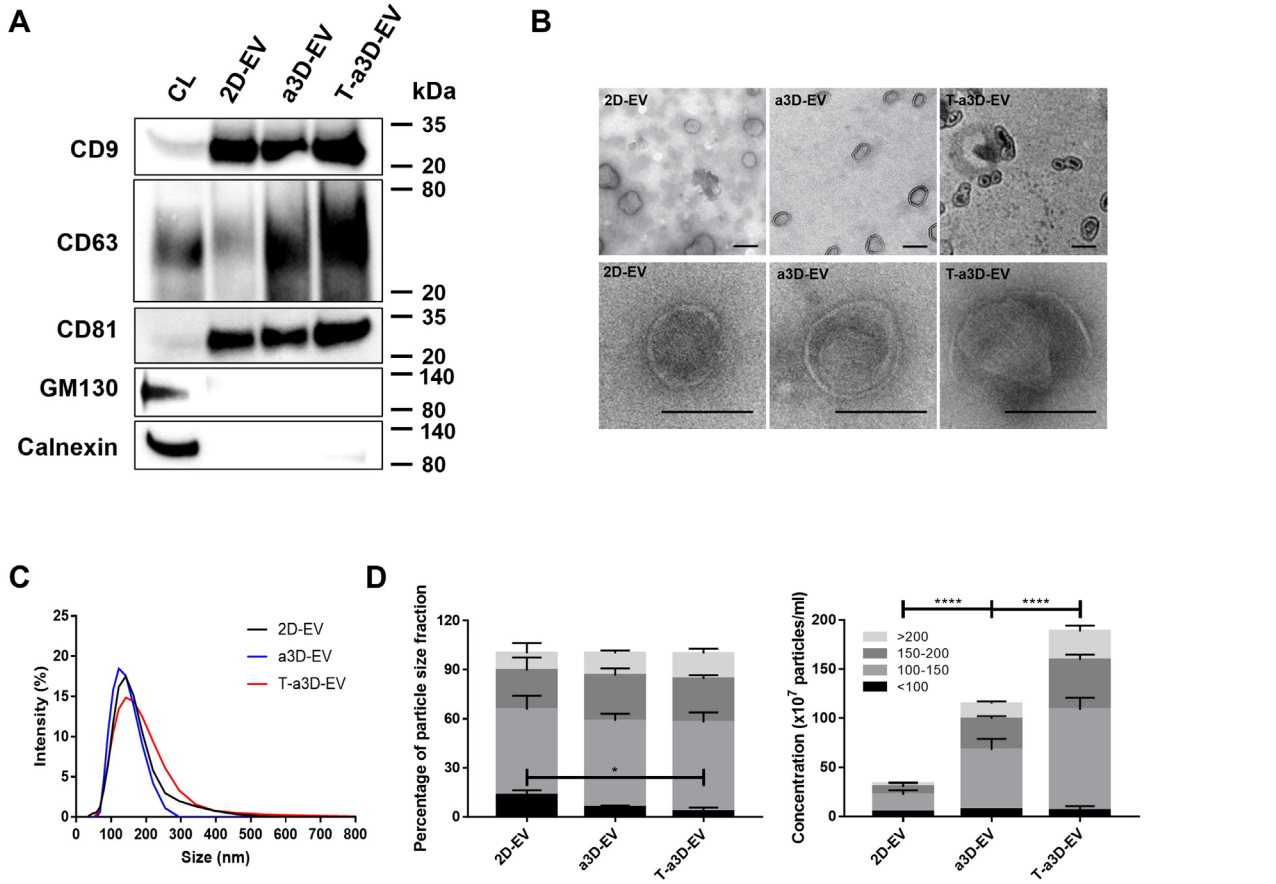

Fig. 4. *Characterization of WJ-MSC-derived a3D-EVs and T-a3D-EVs* (A) Western blot assays for measuring EVs markers (CD9, CD63, and CD81) and negative marker (GM130, Calnexin) expressions in 2D-EVs, a3D-EVs, and T-a3D-EVs. CL: cell lysate. (B) Transmission electron microscopy images of 2D-EVs, a3D-EVs, and T-a3D-EVs with 1 % phosphotungstic acid (upper panel) or 1 % uranyl acetate (bottom panel) negative staining. The scale bars indicate 100 nm. (C) Particle size distribution of 2D-EVs (black), a3D-EVs (blue), and T-a3D-EVs (red) were measured using dynamic light scattering indicating the average size of EVs. (D) Percentage of particle size distribution and concentration of all samples (n = 4). Percentage of size distribution: <100 nm, 100–150 nm, 150–200 nm, >200 nm. Particle concentrations measured per mL. Data are presented as mean ± SEM, and statistical analyses were evaluated by performing two-way ANOVA; $^{*}p < 0.05$ and $^{****}p < 0.0001$.

confirmed that proteins belonging to cluster 2 (increased proteins only in T-a3D-EVs group) were significantly related to tissue regeneration, TGF-β receptor-mediated ECM remodeling, and energy metabolism (Supplementary Table 5).

Moreover, principal component analysis (PCA) was used to identify any inherent trends among the three EV sample sets, revealing that these protein groups were significantly different depending on the culture conditions (2D vs 3D culture) (Component 1: 61.6 %) (Fig. 6D). The differences upon treatment with exogenous TGF-β3 were also clearly reflected in the PCA (Component 2: 27.1 %). Similar to the proteome analysis results with the 2D MSCs, a3D MSC spheroids, or T-a3D MSC spheroids (Fig. 2A), this PCA result for 2D-, a3D-, and T-a3D-EVs indicated that the proteome characteristics of the EVs from 3D-culture conditions (a3D-EVs and T-a3D-EVs) were quite different from those of the 2D-culture conditions (2D-EVs); relatively small proteome changes in T-a3D-EVs may lead to significant enhancement of the EV functional capacity. Consistently, as we attempted to discover the DEPs (FDR of 5 %, $\log_2$(ratio) ≥ 1 or ≤ -1) through pairwise comparisons, the volcano plots of a3D-EVs/2D-EVs and T-a3D-EVs/2D-EVs supported the fact that the number of EV-DEPs (DEPs identified in EVs) caused by the culture conditions (2D and 3D) were apparently higher than those induced by the exogenous TGF-β3 treatment in the T-a3D system (Figure S6C). Furthermore, the volcano plot of T-a3D-EVs vs a3D-EVs revealed that 53 proteins were upregulated, while 14 proteins were downregulated upon exogenous TGF-β3 treatment in the T-a3D system.

Next, as proteins in EVs are generally known to activate various pathways *in vitro* and *in vivo* after internalization into the recipient cells [46–48], we analyzed the predicted roles of the T-3D-EVs-specific DEPs in the EV-treated recipient cells, based on the known molecular and cellular functions of each specific DEP. A Venn diagram was generated using DEPs from the three pairwise comparisons (T-a3D-EVs/2D-EVs, a3D-EVs/2D-EVs, and T-a3D-EVs/a3D-EVs) (Fig. 6E, Supplementary Table 2), showing that the 93 DEPs (40 DEPs from T-a3D-EVs/2D-EVs, 28 DEPs from an overlapping area between the T-a3D-EVs/2D-EVs and T-a3D-EVs/a3D-EVs, and 25 DEPs from T-a3D-EVs/a3D-EVs) could be associated with exogenous TGF-β3 treatment-specific proteins. The 28 proteins from an overlapping area between the T-a3D-EVs/2D-EVs and T-a3D-EVs/a3D-EVs were speculated to be strongly associated with exogenous TGF-β3 treatment but were not affected by the cell culture conditions. The GO analysis of the 28 proteins showed that the proteins were mostly related to cell–cell adhesion, response to ER stress, negative regulation of proteasomal ubiquitin-dependent protein catabolic process, positive regulation of TGF- β receptor signaling, energy producing process and stem cell population maintenance, which can explain regeneration and protein

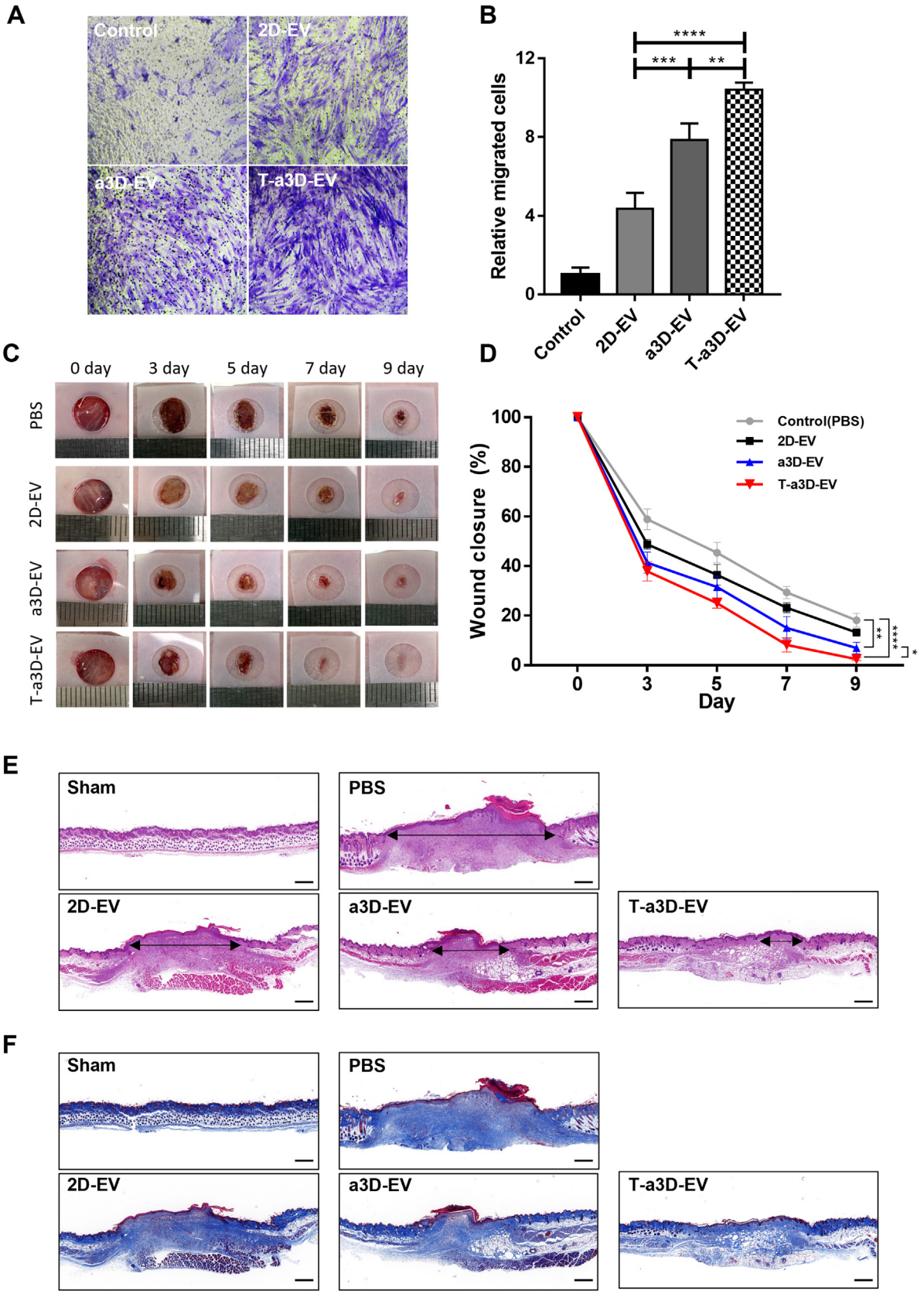

Fig. 5. *The improved wound healing capacity of T-a3D-EVs in vitro and in vivo mouse model* (A) Representative bright-field images of migrated cells on fibroblast indicate a similar number of EVs among the treated a3D-EVs and T-a3D-EVs groups (1×10^8 particles) compared with the 2D-EV-treated controls. Scale bar: 200 μm. (B) Quantitative results from stained cells (migrated cells) were measured using image J software. Data are displayed as mean ± SD (n = 3). Statistical analysis was performed using two-way randomized ANOVA tested for the factors "T-a3D-EVs treated group" and "time", $^{*}p < 0.05$ and $^{****}p < 0.0001$. (C) Representative *in vivo* wound closing images for 0, 3, 5, 7, and 9 days. (D) Quantitative wound closure rate between negative control (PBS) and test groups (EVs). Data are presented as the mean ± standard deviation of three independent experiments. Statistical significance of differences is indicated as follows: $^{*}p < 0.05$, $^{**}p < 0.01$, and $^{****}p < 0.0001$. Representative figure of histological analysis at 9 day using (E) hematoxylin and eosin (H&E) (black arrow; wound length) and (F) Masson's trichrome (MT) staining. Scale bar: 500 μm.

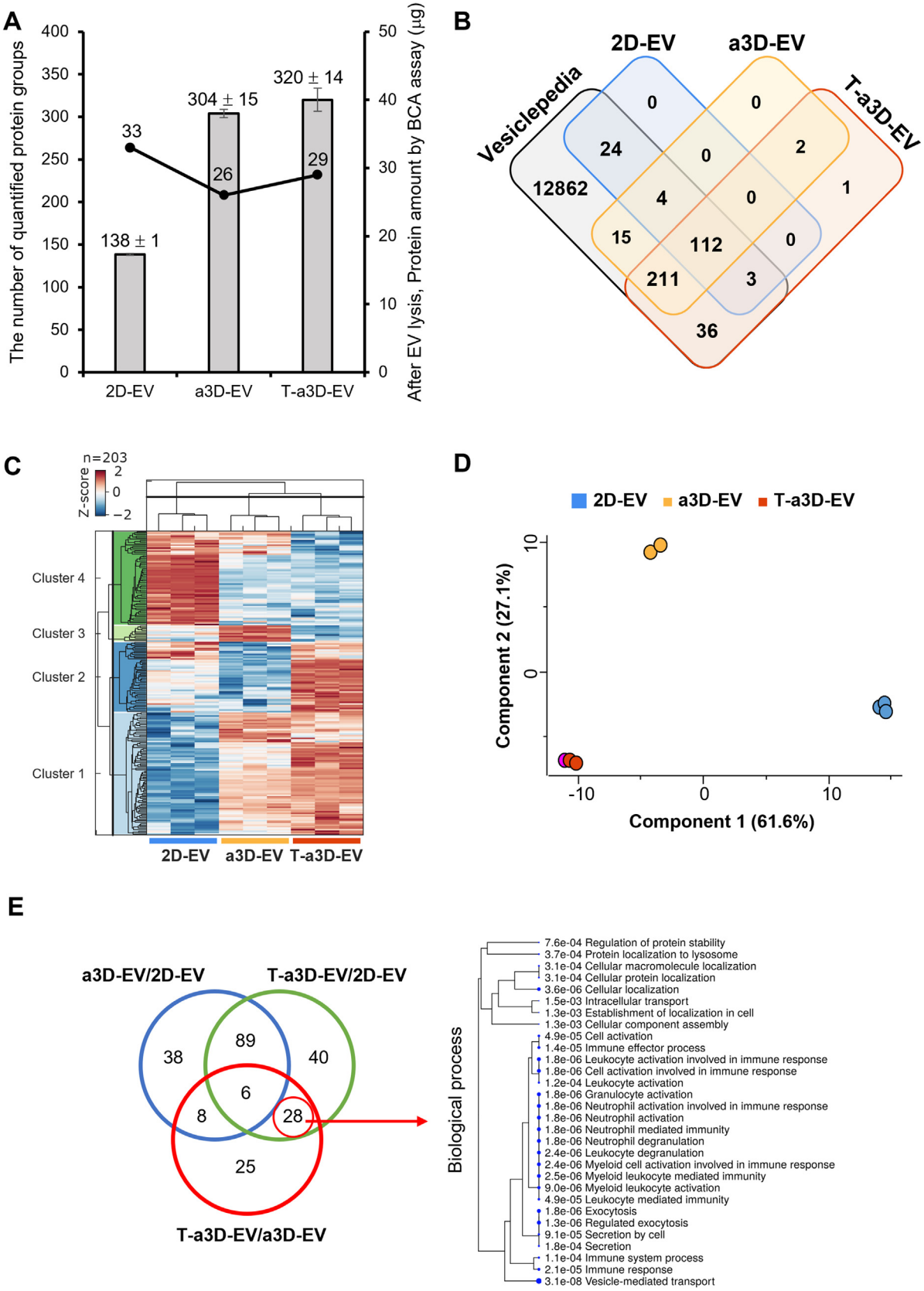
A
The number of quantified protein groups
After EV lysis, Protein amount by BCA assay (μg)
138 ± 1
304 ± 15
320 ± 14
33
26
29
2D-EV
a3D-EV
T-a3D-EV
B
2D-EV
a3D-EV
T-a3D-EV
Vesiclepedia
0
0
24
0
2
12862
4
0
1
15
112
0
211
3
36
C
n=203
Z-score
2
0
−2
Cluster 4
Cluster 3
Cluster 2
Cluster 1
2D-EV
a3D-EV
T-a3D-EV
D
2D-EV
a3D-EV
T-a3D-EV
Component 2 (27.1%)
Component 1 (61.6%)
E
a3D-EV/2D-EV
T-a3D-EV/2D-EV
T-a3D-EV/a3D-EV
38
89
40
6
8
28
25
Biological process
7.6e-04 Regulation of protein stability
3.7e-04 Protein localization to lysosome
3.1e-04 Cellular macromolecule localization
3.1e-04 Cellular protein localization
3.6e-06 Cellular localization
1.5e-03 Intracellular transport
1.3e-03 Establishment of localization in cell
1.3e-03 Cellular component assembly
4.9e-05 Cell activation
1.4e-05 Immune effector process
1.8e-06 Leukocyte activation involved in immune response
1.8e-06 Cell activation involved in immune response
1.2e-04 Leukocyte activation
1.8e-06 Granulocyte activation
1.8e-06 Neutrophil activation involved in immune response
1.8e-06 Neutrophil activation
1.8e-06 Neutrophil mediated immunity
1.8e-06 Neutrophil degranulation
2.4e-06 Leukocyte degranulation
2.4e-06 Myeloid cell activation involved in immune response
2.5e-06 Myeloid leukocyte mediated immunity
9.0e-06 Myeloid leukocyte activation
4.9e-05 Leukocyte mediated immunity
1.8e-06 Exocytosis
1.3e-06 Regulated exocytosis
9.1e-05 Secretion by cell
1.8e-04 Secretion
1.1e-04 Immune system process
2.1e-05 Immune response
3.1e-08 Vesicle-mediated transport

production (Supplementary Table 6) and, among the 28 proteins, expression of F-actin-capping protein subunit alpha-1 was decreased and the other 27 proteins were increased in the T-a3D-EVs.

In silico functional characterization of the DEPs in 2D-, a3D-, and T-a3D-EVs

To examine the functional features of the EVs using EV proteome data, we first performed a gene set enrichment analysis (GSEA) using total DEPs in three EV sample sets. GSEA can reveal whether some groups of proteins that share biological characteristics, such as pathway or gene ontology, can be expressed with statistical significance in two biological statuses. In this study, all DEPs from three exosome sample sets were put into GSEA to find a T-a3D-EV set specific biological pathway compared to other EV sample sets. The results of GSEA between T-a3D-EVs and the other EV samples showed differences in the PI3K-AKT signaling pathway (24 proteins) and the integrin1 (integrin beta-1) pathway (17 proteins) (Fig. 6F, S7).

Among the proteins identified in the PI3K-AKT (24 proteins) and integrin 1 (17 proteins) pathways, 11 proteins were common in both pathways, and out of the 11 proteins, collagen alpha-1 (VI) chain (COL6A1), collagen alpha-3 (VI) chain (COL6A3), and tenascin (TNC) were shown to be significantly enriched only in the T-a3D-EVs. These proteins are involved in ECM remodeling and regeneration. Furthermore, among the 13 proteins found only in the PI3AKT signaling pathway or the six proteins only in the intergrin1 pathway, eukaryotic translation initiation factor 4E (EIF4E), heat shock protein HSP 90-beta (HSP90AB1), endoplasmin (HSP90B1), Ras-related C3 botulinum toxin substrate 1 (RAC1), transforming growth factor beta-1 proprotein (TGF-β1), and protein-glutamine gamma-glutamyltransferase 2 (TGM2) were significantly enriched only in T-a3D-EVs (Fig. 6G). These protein expression patterns related to PI3K-AKT and integrin 1 can promote metabolism, proliferation, cell survival, growth, and angiogenesis in response to extracellular signals, indicating the regeneration effect of T-a3D-EVs on recipient cells.

To identify proteins that interact with our significant protein and to predict their roles and pathways in the recipient cells, the HuRi (Human Reference Protein Interactome Mapping Project) database was analyzed using the identified T-a3D-EV-specific 28 DEPs [49].

As a result, five proteins (protein S100-A10 (S100A10), syntenin-1 (SDCBP), actin, cytoplasmic 2 (ACTG1), PDZ domain-containing protein GIPC1 (GIPC1), and eukaryotic translation initiation factor 4E (EIF4E)) out of the 28 DEPs between the T-a3D-EVs/2D-EVs and T-a3D-EVs/a3D-EVs were shown to interact with 113 interactors in the Huri Database with a confidence score of $\geq$ 0.9 [50] (Fig. 6D, Supplementary Table 7).

Functional annotation of these five DEPs with 113 interactors using the annotation database (ShinyGO v0.61) showed several signaling pathways that could be activated in the recipient cells (Fig. 6H, Supplementary Table 8). One of the related pathways was the regulation of cyclin-dependent protein kinase activity, which supports the potent function of T-a3D-EVs in recipient cells (Supplementary Table 7). In addition, among the DEPs observed in our EV, SDCBP is a type of central protein that primarily interacts with 105 proteins (44.8 %), as shown in Fig. 6H, indicating that SDCBP can be a key regulator of exosome-related effects on recipient cells. SDCBP is involved in immunomodulation, exosome biogenesis, and tumorigenesis [51].

In conclusion, all proteome signatures in T-a3D-EVs compared to other EV sample sets support the regeneration of EMC and immune modulation, as confirmed in our *in vitro* and *in vivo* studies.

Discussion

In this study, we developed a method for the improved production of therapeutically potent EVs with higher yield and efficacy using an advanced 3D culture system and the addition of exogenous TGF-β3. Using this T-a3D method, we can prepare a highly concentrated EV-containing culture medium for efficient EV isolation and purification, which could be applied for minimizing the production time and scale (graphical abstract). We identify frame work for scalable and effective EV production using T-a3D system including the uniformity and optimization of 3D spheroid generation/culture techniques. However, the current production system still has limitations. Isolation methods using ultracentrifuge and gradient ultracentrifuge, even if the iodixanol gradient method is possible to obtain high-purified EVs, are not available for large-scale production. Currently, TFF (Tangential Flow Filtration) is an efficient concentration method for large-scale production of clinical EVs [52]. To purify EVs, size-exclusion chromatography (*SEC*) system is a possible method for clinical approach [13,52,53]. Therefore, T-a3D method should be tested with these purification methods for large-scale production for clinical application.

We previously revealed that mechanical forces induced by hydrodynamic shear stress, applied by repeated shaking and suspension (optimally at 60 rpm; approximately 4 dyne/cm^2), can lead to efficient induction of self-renewal signaling pathways [26]. Here, we confirmed that the MSC spheroids with diameters ranging from 150 to 200 μm displayed homogeneous round shapes at 60 rpm and maintained high expression of stemness and shear stress markers. The mechanical forces applied to MSC spheroids in 3D dynamic culture were reported to modulate multiple signaling pathways via the alteration of MSC morphology, mechanical stress, cell–cell or cell-ECM adhesion capacity, and subsequent conformational changes of cytoskeletal complexes [23–25]. Of particular interest, upregulated TGF-β/Smad2/3 signaling, simultaneously with augmented CD9 expression and EV production, was observed in our a3D and T-a3D dynamic culture systems. While exogenous TGF-β3 treatment in a3D conditions resulted in an increase in EV production, addition of exogenous TGF-β3 in the 2D culture system did not show a significant effect on EV produc-

Fig. 6. *Proteome features of identified EVs proteins from the 2D, a3Ds, and T-a3D conditions* (A) Bar graph indicating the total number of quantified protein groups, and the line plot shows the protein amount by BCA assay after EVs lysis in each sample set. (B) Venn diagram of proteins identified in each EV sample compared with proteins annotated in the Vesiclepedia database. (C) Hierarchical clustering of proteins from each EV sample. Top: sample tree; left: protein tree. Data was grouped by sample type (triplicate analyses per sample), followed by $\log_2$ transformation and ANOVA with Benjamini–Hochberg FDR correction. Data was filtered based on an ANOVA q-value of $\leq$ 0.05. (D) Principal component analysis of the 203 proteins obtained from each EV sample. The two principal components (PC1 and PC2) explaining most of the variation in the dataset are plotted against each other. (E) A Venn diagram indicating the overlap between differentially expressed protein groups. Biological process for 28 proteins significantly observed in T-a3D-EV with red circle. (F) Enrichment score (ES) plots of the PI3K-AKT signaling pathway (upper panel) and integrin beta-1 pathway (lower panel) from GSEA were shown. Positive and negative ES values point to gene sets over-represented in either the up- or down-regulated genes in T-a3D-Evs Vertical bars refer to individual genes in a gene set, and their positions reflect the contribution of each gene to the ES. (G) Heat maps of protein measurements from T-a3D-EVs vs other samples (2D-EV and a3D-EV) depicting relative abundance from red to blue. The upper panel shows the proteins associated with the PI3K-AKT signaling pathway, and the lower panel shows those associated with the integrin beta-1 pathway. (H) HuRi-generated protein–protein interaction networks for 28 significant proteins in T-a3D-EV with 234 interactors was shown as network. Red circles with yellow letters are DEPs from EV proteome analysis from this study and blue circles with white letters are the interactor proteins from HuRi database and black lines between circle indicate interaction.

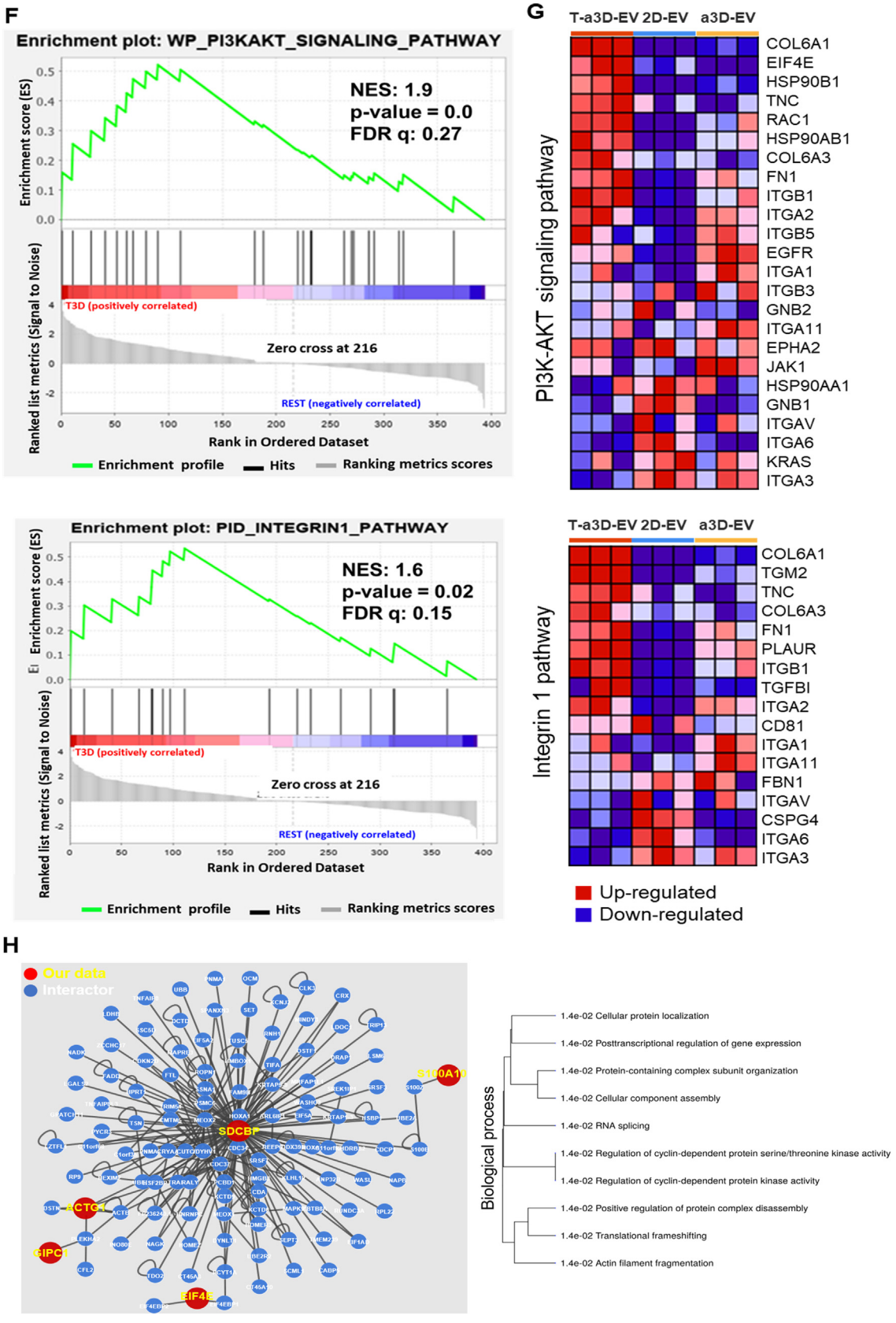

Fig. 6 (*continued*)

tion (Figure S3), implying that exogenous TGF-β3 in 2D culture conditions may not be sufficient to enhance EV production. Importantly, in both a3D and T-a3D systems, treatment with TGF-β receptor inhibitors led to an apparent suppression of CD9 expression (mRNA and protein) along with a significant decrease in EV production, strongly suggesting that the dynamic 3D culture- and

exogenous TGF-β3-induced TGF-β signaling pathway in a3D and T-a3D systems may play a very important role in enhancing this production.

Of note, our quantitative proteomic analysis of the T-a3D spheroids and T-a3D-EVs could support the TGF-β signaling-mediated improvement of EV production as well as the high *in vitro* and *in vivo* therapeutic potency of T-a3D-EVs. In our quantitative proteomic analysis of the MSC spheroids, an interesting observation was that most of the DEPs in a3D and T-a3D spheroids were associated with exocytosis, supporting that the proteins affected by the dynamic 3D culture- and exogenous TGF-β3-induced TGF-β signaling pathway in a3D and T-a3D systems have a crucial influence on the enhanced EV production. Moreover, a comprehensive proteomic analysis of EVs revealed that EV production in a3D or T-a3D systems was influenced by secreted paracrine factors including TGF-β, fibroblast growth factor 1 (FGF1), vascular endothelial growth factor (VEGF), and prostaglandin E2 (PGE2) [54–56], supporting the importance of the autocrine effect.

Under certain conditions, TGF-β3 has been reported to induce MSCs into chondrocytes [57,58] and TGF-β3 mixed with other factors in the chondrogenic differentiation medium could act as a chondrogenic factor. Moreover, 3D spheroid condition can induce differentiation capacity of stem cells. [17,39]. However, both the dynamic culture in the a3D system and TGF-β3 treatment in the T-a3D system led to enhanced expression of the stemness-related genes (OCT4, SOX2, and Krüppel-like factor-4) and proteins (OCT4, SOX2, and Nanog), suggesting that the dynamic 3D culture- and exogenous TGF-β3-induced TGF-β signaling pathway in a3D and T-a3D systems may play a significant role in the maintenance of MSC stemness. Further studies are underway to elucidate the detailed mechanism by which TGF-β3 under our dynamic culture conditions may play a role in stemness maintenance rather than chondrogenesis.

We hypothesized that T-a3D-EVs could enhance therapeutic effects by affecting their therapeutic cargo content. To evaluate the functional effects of EVs, we conducted an experiment to compare the effects of 2D-, a3D-, and T-a3D-EVs in an *in vivo* wound healing model. *In vitro* migration assays of dermal fibroblasts showed a higher migration effect in the T-a3D-EVs treated group compared than in the other groups. The results of the full-thickness excisional wound model showed a positive correlation with the *in vitro* studies, indicating a significant wound healing effect of T-a3D-EVs. TGF-β3 has effects on wound healing processes, including regeneration and anti-inflammation. To exclude the role of the possible contamination of TGF-β3 in the final EVs, we performed bottom-up purification using iodixanol and confirmed that the residual amounts of TGF-β3 were hardly detected in T-a3D-EVs, supporting the enhanced therapeutic effect of T-a3D-EVs cargos.

The therapeutic effects of T-a3D-EVs are only tested for the excision wound healing model. Further study will be needed to investigate therapeutic effects for various diseases specifically with animal disease models already known for EV efficacy such as the anti-inflammatory and regenerative effects of T-a3D-EVs on injured or degenerative disease models including including myocardial ischemia/reperfusion (I/R) injury, graft-versus-host-disease, osteoarthritis, sepsis, stroke and Alzheimer's disease [59]. The proteomic approach in this study enabled us to characterize the proteins in EVs and infer their related signaling pathways. Here, a well-curated database of protein–protein interactions (HuRi database) analysis and a computational method (GSEA) were applied to predict the functions and the pathways involved in the EV proteins in the recipient cells. Interestingly, T-a3D-EVs cargos were particularly rich in proteins related to the PI3K-AKT signaling pathway and the integrin1 pathway, which are well known to be involved in wound healing mechanisms, including regeneration [60,61] and anti-inflammatory [62,63]. In addition, T-a3D-EVs are rich in SDCBP, which is known to be involved in immunomodulation, exosome biogenesis, and tumorigenesis [51]. Further, through interaction analysis, we confirmed that SDCBP, Syntenin-1 were especially rich in T-a3D-EVs, implying that the regulation of cyclin-dependent protein kinase activity may be involved in the enhanced therapeutic effect of T-a3D-EVs. CDC37, which has been reported to play a major role in tissue regeneration [64], may be a crucial factor for wound healing and JNK pathway activation for the enhanced therapeutic effect of T-a3D-EVs. Although there are limitations in speculating the expected functions along with culture conditions as many proteins were identified at the cellular level, proteomic analysis was useful to identify the proteins that play an important role in the enhanced therapeutic effects of T-a3D-EVs, verifying that the proteome analysis of EV cargos has the advantage of speculating their therapeutic potential.

Conclusion

In summary, our results reveal that T-a3D conditions can boost the production of therapeutically potent EVs through dynamic culture (mechanical force) and exogenous TGF-β-mediated upregulation of TGF-β signaling and CD9 expression. Comprehensive proteomic analysis revealed that the EVs produced under T-a3D were particularly rich in protein cargo with high therapeutic potential.

Compliance with ethics requirements

The protocols used in this study were approved by the ethics committees of Konkuk University (7001355–202010-BR-407) and IACUC at Konkuk University (KU20132-1) and conformed to the principles outlined in the Declaration of Helsinki.

CRediT authorship contribution statement

Kyung Min Lim: Conceptualization, Methodology, Investigation, Data curation, Supervision, Project administration, Funding acquisition. **Sehee Kim:** Conceptualization, Methodology, Formal analysis, Investigation, Resources, Data curation, Visualization. **Jeonghun Yeom:** Conceptualization, Formal analysis, Investigation, Resources, Data curation, Visualization. **Yujin Choi:** Methodology, Resources. **Yoonjoo Lee:** Validation, Data curation. **Jongyub An:** Formal analysis, Visualization. **Minchan Gil:** Methodology, Validation, Data curation. **Ahmed Abdal Dayem:** Resources. **Kyeongseok Kim:** . **Geun-Ho Kang:** Methodology, Validation. **Aram Kim:** Investigation, Visualization. **Kwonho Hong:** Validation, Data curation. **Kyunggon Kim:** Methodology, Resources. **Ssang-Goo Cho:** Conceptualization, Methodology, Investigation, Validation, Data curation, Supervision, Project administration, Funding acquisition.

Declaration of Competing Interest

S-G.C. was a StemExOne stockholder. K.M.L. and G-H.K. are employed by StemExOne Ltd. The other authors declare that they have no known competing financial interests or personal relationships that could have appeared to influence the work reported in this paper.

Acknowledgement

This study was supported by a grant from the National Research Foundation (NRF) funded by the Korean Government (Grant No. 2019M3A9H1030682), Korean Fund for Regenerative Medicine funded by Ministry of Science and ICT, and Ministry of Health and Welfare (Grant No. 22B0502L1-01), Samsung Research Fund-

ing and Incubation Center for Future Technology (Grant No. SRFCIT1802-03) and funded by a cooperative research program of rural development administration (#PJ015336012021). We would like to thank Editage (www.editage.co.kr) for English language editing.

Appendix A. Supplementary data

Supplementary data to this article can be found online at https://doi.org/10.1016/j.jare.2022.09.005.

References

[1] Lötvall J, Hill AF, Hochberg F, Buzás EI, Di Vizio D, Gardiner C, et al. Minimal experimental requirements for definition of extracellular vesicles and their functions: a position statement from the International Society for Extracellular Vesicles. Taylor & Francis; 2014.
[2] Yáñez-Mó M, Siljander PR-M, Andreu Z, Bedina Zavec A, Borràs FE, Buzas EI, et al. Biological properties of extracellular vesicles and their physiological functions. Journal of extracellular vesicles. 2015;4(1):27066.
[3] Valadi H, Ekström K, Bossios A, Sjöstrand M, Lee JJ, Lötvall JO. Exosome-mediated transfer of mRNAs and microRNAs is a novel mechanism of genetic exchange between cells. Nat Cell Biol 2007;9(6):654–9.
[4] Wu P, Zhang B, Ocansey DKW, Xu W. Qian H. Extracellular vesicles: A bright star of nanomedicine. Biomaterials; 2020. p. 120467.
[5] Stephen J, Bravo EL, Colligan D, Fraser AR, Petrik J, Campbell JD. Mesenchymal stromal cells as multifunctional cellular therapeutics–a potential role for extracellular vesicles. Transfus Apheres Sci 2016;55(1):62–9.
[6] L PK, Kandoi S, Misra R, S V, K R, Verma RS. The mesenchymal stem cell secretome: A new paradigm towards cell-free therapeutic mode in regenerative medicine. Cytokine Growth Factor Rev. 2019;46:1-9.
[7] Wei Y, Wu Y, Zhao R, Zhang K, Midgley AC, Kong D, et al. MSC-derived sEVs enhance patency and inhibit calcification of synthetic vascular grafts by immunomodulation in a rat model of hyperlipidemia. Biomaterials 2019;204:13–24.
[8] van Dommelen SM, Vader P, Lakhal S, Kooijmans S, van Solinge WW, Wood MJ, et al. Microvesicles and exosomes: opportunities for cell-derived membrane vesicles in drug delivery. J Control Release 2012;161(2):635–44.
[9] Phinney DG, Pittenger MF. Concise review: MSC-derived exosomes for cell-free therapy. Stem cells 2017;35(4):851–8.
[10] Burnley-Hall N, Willis G, Davis J, Rees DA, James PE. Nitrite-derived nitric oxide reduces hypoxia-inducible factor 1α-mediated extracellular vesicle production by endothelial cells. Nitric Oxide 2017;63:1–12.
[11] Ti D, Hao H, Tong C, Liu J, Dong L, Zheng J, et al. LPS-preconditioned mesenchymal stromal cells modify macrophage polarization for resolution of chronic inflammation via exosome-shuttled let-7b. Journal of translational medicine 2015;13(1):308.
[12] Sung DK, Chang YS, Sung SI, Ahn SY, Park WS. Thrombin preconditioning of extracellular vesicles derived from mesenchymal stem cells accelerates cutaneous wound healing by boosting their biogenesis and enriching cargo content. Journal of clinical medicine 2019;8(4):533.
[13] Haraszti RA, Miller R, Stoppato M, Sere YY, Coles A, Didiot M-C, et al. Exosomes produced from 3D cultures of MSCs by tangential flow filtration show higher yield and improved activity. Mol Ther 2018;26(12):2838–47.
[14] Kim M, Yun H-W, Choi BH, Min B-H. Three-dimensional spheroid culture increases exosome secretion from mesenchymal stem cells. Tissue engineering and regenerative medicine 2018;15(4):427–36.
[15] Kim ES, Kida K, Mok J, Seong Y, Jo SY, Kanaki T, et al. Cellhesion VP enhances the immunomodulating potential of human mesenchymal stem cell-derived extracellular vesicles. Biomaterials. 2021;271:120742.
[16] Lim KM, Dayem AA, Choi Y, Lee Y, An J, Gil M, et al. High Therapeutic and Esthetic Properties of Extracellular Vesicles Produced from the Stem Cells and Their Spheroids Cultured from Ocular Surgery-Derived Waste Orbicularis Oculi Muscle Tissues. Antioxidants 2021;10(8):1292.
[17] Sart S, Tsai A-C, Li Y, Ma T. Three-dimensional aggregates of mesenchymal stem cells: cellular mechanisms, biological properties, and applications. Tissue Engineering Part B: Reviews 2014;20(5):365–80.
[18] Bartosh TJ, Ylöstalo JH, Mohammadipoor A, Bazhanov N, Coble K, Claypool K, et al. Aggregation of human mesenchymal stromal cells (MSCs) into 3D spheroids enhances their antiinflammatory properties. Proc Natl Acad Sci 2010;107(31):13724–9.
[19] Frith JE, Thomson B, Genever PG. Dynamic three-dimensional culture methods enhance mesenchymal stem cell properties and increase therapeutic potential. Tissue Engineering Part C: Methods 2010;16(4):735–49.
[20] Cao J, Wang B, Tang T, Lv L, Ding Z, Li Z, et al. Three-dimensional culture of MSCs produces exosomes with improved yield and enhanced therapeutic efficacy for cisplatin-induced acute kidney injury. Stem Cell Res Ther 2020;11(1):1–13.
[21] YlÖstalo JH, Bartosh TJ, Coble K, Prockop DJ. Human mesenchymal stem/stromal cells cultured as spheroids are self-activated to produce prostaglandin E2 that directs stimulated macrophages into an anti-inflammatory phenotype. Stem cells 2012;30(10):2283–96.
[22] Petrenko Y, Syková E, Kubinová Š. The therapeutic potential of three-dimensional multipotent mesenchymal stromal cell spheroids. Stem Cell Res Ther 2017;8(1):94.
[23] MacQueen L, Sun Y, Simmons CA. Mesenchymal stem cell mechanobiology and emerging experimental platforms. J R Soc Interface 2013;10(84):20130179.
[24] Wang J, Thampatty B. Chapter 7 Mechanobiology of Adult and Stem Cells International review of cell and molecular biology 2008;271:301–46.
[25] Vermeulen S, Roumans N, Honig F, Carlier A, Hebels DG, Eren AD, et al. Mechanotransduction is a context-dependent activator of TGF-β signaling in mesenchymal stem cells. Biomaterials. 2020;259:120331.
[26] Choi HY, Yang GM, Dayem AA, Saha SK, Kim K, Yoo Y, et al. Hydrodynamic shear stress promotes epithelial-mesenchymal transition by downregulating ERK and GSK3beta activities. Breast Cancer Res 2019;21(1):6.
[27] Malek AM, Alper SL, Izumo S. Hemodynamic shear stress and its role in atherosclerosis. JAMA 1999;282(21):2035–42.
[28] Choi HY, Yang G-M, Dayem AA, Saha SK, Kim K, Yoo Y, et al. Hydrodynamic shear stress promotes epithelial-mesenchymal transition by downregulating ERK and GSK3β activities. Breast Cancer Res 2019;21(1):1–20.
[29] Reneman RS, Hoeks AP. Wall shear stress as measured in vivo: consequences for the design of the arterial system. Med Biol Eng Compu 2008;46(5):499–507.
[30] Saha SK, Choi HY, Yang G-M, Biswas PK, Kim K, Kang G-H, et al. GPR50 promotes hepatocellular carcinoma progression via the Notch signaling pathway through direct interaction with ADAM17. Molecular Therapy-Oncolytics 2020;17:332–49.
[31] Wojciech S, Ahmad R, Belaid-Choucair Z, Journé A-S, Gallet S, Dam J, et al. The orphan GPR50 receptor promotes constitutive TGFβ receptor signaling and protects against cancer development. Nat Commun 2018;9(1):1–15.
[32] Maeda T, Sakabe T, Sunaga A, Sakai K, Rivera AL, Keene DR, et al. Conversion of mechanical force into TGF-β-mediated biochemical signals. Curr Biol 2011;21(11):933–41.
[33] Walshe TE, dela Paz NG, D'Amore PA. The role of shear-induced transforming growth factor-β signaling in the endothelium. Arteriosclerosis, thrombosis, and vascular biology. 2013;33(11):2608-17.
[34] Abuammah A, Maimari N, Towhidi L, Frueh J, Chooi KY, Warboys C, et al. New developments in mechanotransduction: Cross talk of the Wnt, TGF-β and Notch signalling pathways in reaction to shear stress. Current Opinion in Biomedical Engineering 2018;5:96–104.
[35] Cha JM, Shin EK, Sung JH, Moon GJ, Kim EH, Cho YH, et al. Efficient scalable production of therapeutic microvesicles derived from human mesenchymal stem cells. Sci Rep 2018;8(1):1–16.
[36] Shelke GV, Lässer C, Gho YS, Lötvall J. Importance of exosome depletion protocols to eliminate functional and RNA-containing extracellular vesicles from fetal bovine serum. Journal of extracellular vesicles 2014;3(1):24783.
[37] Lobb RJ, Becker M, Wen Wen S, Wong CS, Wiegmans AP, Leimgruber A, et al. Optimized exosome isolation protocol for cell culture supernatant and human plasma. Journal of extracellular vesicles 2015;4(1):27031.
[38] Greening DW, Xu R, Ji H, Tauro BJ, Simpson RJ. A protocol for exosome isolation and characterization: evaluation of ultracentrifugation, density-gradient separation, and immunoaffinity capture methods. Proteomic Profiling: Springer; 2015. p. 179–209.
[39] Dahlin RL, Ni M, Meretoja VV, Kasper FK, Mikos AG. TGF-β3-induced chondrogenesis in co-cultures of chondrocytes and mesenchymal stem cells on biodegradable scaffolds. Biomaterials 2014;35(1):123–32.
[40] Ostrowski M, Carmo NB, Krumeich S, Fanget I, Raposo G, Savina A, et al. Rab27a and Rab27b control different steps of the exosome secretion pathway. Nat Cell Biol 2010;12(1):19–30.
[41] Bobrie A, Krumeich S, Reyal F, Recchi C, Moita LF, Seabra MC, et al. Rab27a supports exosome-dependent and-independent mechanisms that modify the tumor microenvironment and can promote tumor progression. Cancer Res 2012;72(19):4920–30.
[42] Szklarczyk D, Franceschini A, Wyder S, Forslund K, Heller D, Huerta-Cepas J, et al. STRING v10: protein–protein interaction networks, integrated over the tree of life. Nucleic acids research. 2015;43(D1):D447-D52.
[43] Shi Y, Massagué J. Mechanisms of TGF-β signaling from cell membrane to the nucleus. Cell 2003;113(6):685–700.
[44] Keerthikumar S, Chisanga D, Ariyaratne D, Al Saffar H, Anand S, Zhao K, et al. ExoCarta: a web-based compendium of exosomal cargo. J Mol Biol 2016;428(4):688–92.
[45] Kalra H, Simpson RJ, Ji H, Aikawa E, Altevogt P, Askenase P, et al. Vesiclepedia: a compendium for extracellular vesicles with continuous community annotation. PLoS Biol. 2012;10(12):e1001450.
[46] Van Niel G, d'Angelo G, Raposo G. Shedding light on the cell biology of extracellular vesicles. Nat Rev Mol Cell Biol 2018;19(4):213.
[47] Mathieu M, Martin-Jaular L, Lavieu G, Thery C. Specificities of secretion and uptake of exosomes and other extracellular vesicles for cell-to-cell communication. Nat Cell Biol 2019;21(1):9–17.
[48] Raimondo S, Giavaresi G, Lorico A, Alessandro R. Extracellular vesicles as biological shuttles for targeted therapies. Int J Mol Sci 2019;20(8):1848.
[49] Luck K, Kim D-K, Lambourne L, Spirohn K, Begg BE, Bian W, et al. A reference map of the human binary protein interactome. Nature 2020;580(7803):402–8.
[50] Braun P, Tasan M, Dreze M, Barrios-Rodiles M, Lemmens I, Yu H, et al. An experimentally derived confidence score for binary protein-protein interactions. Nat Methods 2009;6(1):91.

[51] Philley JV, Kannan A, Dasgupta S. MDA-9/Syntenin Control. J Cell Physiol 2016;231(3):545–50.
[52] Clos-Sansalvador M, Monguió-Tortajada M, Roura S, Franquesa M, Borràs FE. Commonly used methods for extracellular vesicles' enrichment: Implications in downstream analyses and use. Eur J Cell Biol 2022;151227.
[53] Busatto S, Vilanilam G, Ticer T, Lin WL, Dickson DW, Shapiro S, et al. Tangential Flow Filtration for Highly Efficient Concentration of Extracellular Vesicles from Large Volumes of Fluid. Cells 2018;7(12).
[54] Petrenko Y, Syková E, Kubinová Š. The therapeutic potential of three-dimensional multipotent mesenchymal stromal cell spheroids. Stem Cell Res Ther 2017;8(1):1–9.
[55] Zimmermann JA, Mcdevitt TC. Pre-conditioning mesenchymal stromal cell spheroids for immunomodulatory paracrine factor secretion. Cytotherapy 2014;16(3):331–45.
[56] Han H-W, Asano S, Hsu S-h. Cellular spheroids of mesenchymal stem cells and their perspectives in future healthcare. Applied Sciences 2019;9(4):627..
[57] Thorpe SD, Buckley CT, Vinardell T, O'Brien FJ, Campbell VA, Kelly DJ. The response of bone marrow-derived mesenchymal stem cells to dynamic compression following TGF-β3 induced chondrogenic differentiation. Ann Biomed Eng 2010;38(9):2896–909.
[58] Gupta MS, Nicoll SB. Duration of TGF-β3 exposure impacts the chondrogenic maturation of human MSCs in photocrosslinked carboxymethylcellulose hydrogels. Ann Biomed Eng 2015;43(5):1145–57.
[59] Toh WS, Lai RC, Zhang B, Lim SK. MSC exosome works through a protein-based mechanism of action. Biochem Soc Trans 2018;46(4):843–53.
[60] Zhang W, Bai X, Zhao B, Li Y, Zhang Y, Li Z, et al. Cell-free therapy based on adipose tissue stem cell-derived exosomes promotes wound healing via the PI3K/Akt signaling pathway. Exp Cell Res 2018;370(2):333–42.
[61] Zhang J, Liu X, Li H, Chen C, Hu B, Niu X, et al. Exosomes/tricalcium phosphate combination scaffolds can enhance bone regeneration by activating the PI3K/Akt signaling pathway. Stem Cell Res Ther 2016;7(1):1–14.
[62] Antonov AS, Antonova GN, Munn DH, Mivechi N, Lucas R, Catravas JD, et al. αVβ3 integrin regulates macrophage inflammatory responses via PI3 kinase/Akt-dependent NF-κB activation. J Cell Physiol 2011;226(2):469–76.
[63] Brooke G, Tong H, Levesque J-P, Atkinson K. Molecular trafficking mechanisms of multipotent mesenchymal stem cells derived from human bone marrow and placenta. Stem Cells Dev 2008;17(5):929–40.
[64] Lee C-w, Kwon Y-C, Lee Y, Park M-Y, Choe K-M. cdc37 is essential for JNK pathway activation and wound closure in Drosophila. Molecular biology of the cell. 2019;30(21):2651-8.